

CHAPTER 49

SOLAR ENERGY APPLICATIONS

Jan F. Kreider

**Jan F. Kreider and Associates, Inc.
and Joint Center for Energy Management
University of Colorado
Boulder, Colorado**

49.1 SOLAR ENERGY AVAILABILITY	1549	49.3.2 Mechanical Solar Space Heating Systems	1569
49.1.1 Solar Geometry	1549	49.3.3 Passive Solar Space Heating Systems	1571
49.1.2 Sunrise and Sunset	1552	49.3.4 Solar Ponds	1571
49.1.3 Quantitative Solar Flux Availability	1554	49.3.5 Industrial Process Applications	1575
49.2 SOLAR THERMAL COLLECTORS	1560	49.3.6 Solar Thermal Power Production	1575
49.2.1 Flat-Plate Collectors	1560	49.3.7 Other Thermal Applications	1576
49.2.2 Concentrating Collectors	1564	49.3.8 Performance Prediction for Solar Thermal Processes	1576
49.2.3 Collector Testing	1568		
49.3 SOLAR THERMAL APPLICATIONS	1569	49.4 NONTHERMAL SOLAR ENERGY APPLICATIONS	1577
49.3.1 Solar Water Heating	1569		

49.1 SOLAR ENERGY AVAILABILITY

Solar energy is defined as that radiant energy transmitted by the sun and intercepted by earth. It is transmitted through space to earth by electromagnetic radiation with wavelengths ranging between 0.20 and 15 microns. The availability of solar flux for terrestrial applications varies with season, time of day, location, and collecting surface orientation. In this chapter we shall treat these matters analytically.

49.1.1 Solar Geometry

Two motions of the earth relative to the sun are important in determining the intensity of solar flux at any time—the earth's rotation about its axis and the annual motion of the earth and its axis about the sun. The earth rotates about its axis once each day. A solar day is defined as the time that elapses between two successive crossings of the local meridian by the sun. The local meridian at any point is the plane formed by projecting a north-south longitude line through the point out into space from the center of the earth. The length of a solar day on the average is slightly less than 24 hr, owing to the forward motion of the earth in its solar orbit. Any given day will also differ from the average day owing to orbital eccentricity, axis precession, and other secondary effects embodied in the equation of time described below.

Declination and Hour Angle

The earth's orbit about the sun is elliptical with eccentricity of 0.0167. This results in variation of solar flux on the outer atmosphere of about 7% over the course of a year. Of more importance is the variation of solar intensity caused by the inclination of the earth's axis relative to the ecliptic plane of the earth's orbit. The angle between the ecliptic plane and the earth's equatorial plane is 23.45°. Figure 49.1 shows this inclination schematically.

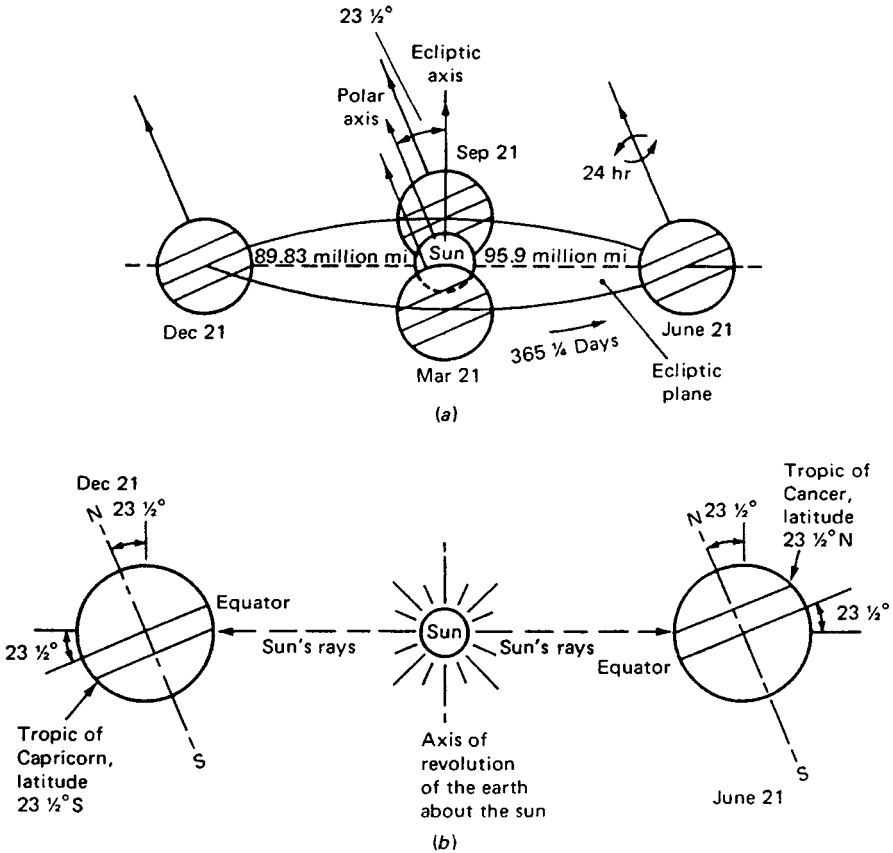


Fig. 49.1 (a) Motion of the earth about the sun. (b) Location of tropics. Note that the sun is so far from the earth that all the rays of the sun may be considered as parallel to one another when they reach the earth.

The earth's motion is quantified by two angles varying with season and time of day. The angle varying on a seasonal basis that is used to characterize the earth's location in its orbit is called the solar "declination." It is the angle between the earth-sun line and the equatorial plane as shown in Fig. 49.2. The declination δ_s is taken to be positive when the earth-sun line is north of the equator and negative otherwise. The declination varies between $+23.45^\circ$ on the summer solstice (June 21 or 22) and -23.45° on the winter solstice (December 21 or 22). The declination is given by

$$\sin \delta_s = 0.398 \cos [0.986(N - 173)] \quad (49.1)$$

in which N is the day number.

The second angle used to locate the sun is the solar-hour angle. Its value is based on the nominal 360° rotation of the earth occurring in 24 hr. Therefore, 1 hr is equivalent to an angle of 15° . The hour angle is measured from zero at solar noon. It is denoted by h_s and is positive before solar noon and negative after noon in accordance with the right-hand rule. For example 2:00 PM corresponds to $h_s = -30^\circ$ and 7:00 AM corresponds to $h_s = +75^\circ$.

Solar time, as determined by the position of the sun, and clock time differ for two reasons. First, the length of a day varies because of the ellipticity of the earth's orbit; and second, standard time is determined by the standard meridian passing through the approximate center of each time zone. Any position away from the standard meridian has a difference between solar and clock time given by $[(\text{local longitude} - \text{standard meridian longitude})/15]$ in units of hours. Therefore, solar time and local standard time (LST) are related by

$$\text{solar time} = \text{LST} - \text{EoT} - (\text{local longitude} - \text{standard meridian longitude})/15 \quad (49.2)$$

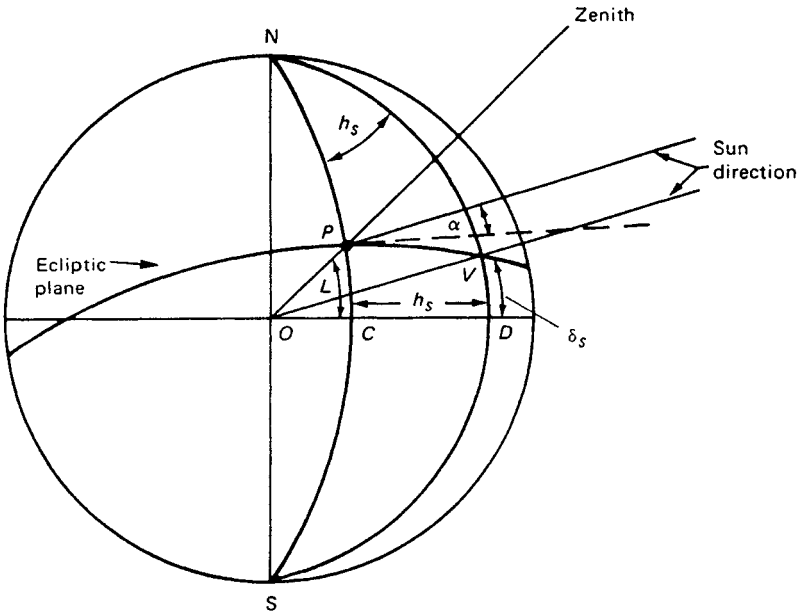


Fig. 49.2 Definition of solar-hour angle h_s (CND), solar declination δ_s (VOD), and latitude L (POC): P , site of interest. (Modified from J. F. Kreider and F. Kreith, *Solar Heating and Cooling*, revised 1st ed., Hemisphere, Washington, DC, 1977.)

in units of hours. EoT is the equation of time which accounts for difference in day length through a year and is given by

$$\text{EoT} = 12 + 0.1236 \sin x - 0.0043 \cos x + 0.1538 \sin 2x + 0.0608 \cos 2x \quad (49.3)$$

in units of hours. The parameter x is

$$x = \frac{360(N - 1)}{365.24} \quad (49.4)$$

where N is the day number counted from January 1 as $N = 1$.

Solar Position

The sun is imagined to move on the celestial sphere, an imaginary surface centered at the earth's center and having a large but unspecified radius. Of course, it is the earth that moves, not the sun, but the analysis is simplified if one uses this Ptolemaic approach. No error is introduced by the moving sun assumption, since the relative motion is the only motion of interest. Since the sun moves on a spherical surface, two angles are sufficient to locate the sun at any instant. The two most commonly used angles are the solar-altitude and azimuth angles (see Fig. 49.3) denoted by α and a_s , respectively. Occasionally, the solar-zenith angle, defined as the complement of the altitude angle, is used instead of the altitude angle.

The solar-altitude angle is related to the previously defined declination and hour angles by

$$\sin \alpha = \cos L \cos \delta_s \cos h_s + \sin L \sin \delta_s \quad (49.5)$$

in which L is the latitude, taken positive for sites north of the equator and negative for sites south of the equator. The altitude angle is found by taking the inverse sine function of Eq. (49.5).

The solar-azimuth angle is given by¹

$$\sin a_s = \frac{\cos \delta_s \sin h_s}{\cos \alpha} \quad (49.6)$$

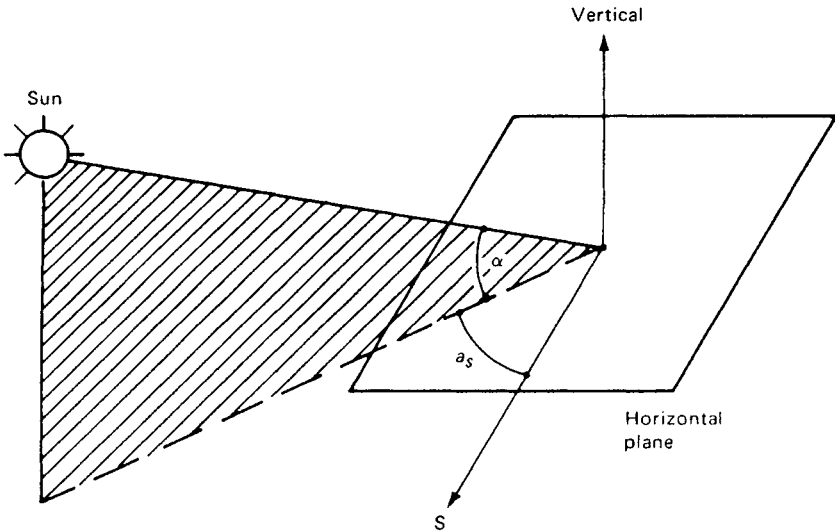


Fig. 49.3 Diagram showing solar-altitude angle α and solar-azimuth angle a_s .

To find the value of a_s , the location of the sun relative to the east-west line through the site must be known. This is accounted for by the following two expressions for the azimuth angle:

$$a_s = \sin^{-1} \left(\frac{\cos \delta_s \sin h_s}{\cos \alpha} \right), \quad \cos h_s > \frac{\tan \delta_s}{\tan L} \quad (49.7)$$

$$a_s = 180^\circ - \sin^{-1} \left(\frac{\cos \delta_s \sin h_s}{\cos \alpha} \right), \quad \cos h_s < \frac{\tan \delta_s}{\tan L} \quad (49.8)$$

Table 49.1 lists typical values of altitude and azimuth angles for latitude $L = 40^\circ$. Complete tables are contained in Refs. 1 and 2.

49.1.2 Sunrise and Sunset

Sunrise and sunset occur when the altitude angle $\alpha = 0$. As indicated in Fig. 49.4, this occurs when the center of the sun intersects the horizon plane. The hour angle for sunrise and sunset can be found from Eq. (49.5) by equating α to zero. If this is done, the hour angles for sunrise and sunset are found to be

$$h_{sr} = \cos^{-1}(-\tan L \tan \delta_s) = -h_{ss} \quad (49.9)$$

in which h_{sr} is the sunrise hour angle and h_{ss} is the sunset hour angle.

Figure 49.4 shows the path of the sun for the solstices and the equinoxes (length of day and night are both 12 hr on the equinoxes). This drawing indicates the very different azimuth and altitude angles that occur at different times of year at identical clock times. The sunrise and sunset hour angles can be read from the figures where the sun paths intersect the horizon plane.

Solar Incidence Angle

For a number of reasons, many solar collection surfaces do not directly face the sun continuously. The angle between the sun–earth line and the normal to any surface is called the incidence angle. The intensity of off-normal solar radiation is proportional to the cosine of the incidence angle. For example, Fig. 49.5 shows a fixed planar surface with solar radiation intersecting the plane at the incidence angle i measured relative to the surface normal. The intensity of flux at the surface is $I_b \times \cos i$, where I_b is the beam radiation along the sun–earth line; I_b is called the direct, normal radiation. For a fixed surface such as that in Fig. 49.5 facing the equator, the incidence angle is given by

$$\begin{aligned} \cos i &= \sin \delta_s (\sin L \cos \beta - \cos L \sin \beta \cos a_w) \\ &+ \cos \delta_s \cos h_s (\cos L \cos \beta + \sin L \sin \beta \cos a_w) \\ &+ \cos \delta_s \sin \beta \sin a_w \sin h_s \end{aligned} \quad (49.10)$$

Table 49.1 Solar Position for 40°N Latitude

Date	Solar Time		Solar Position		Date	Solar Time		Solar Position	
	AM	PM	Altitude	Azimuth		AM	PM	Altitude	Azimuth
January 21	8	4	8.1	55.3	July 21	5	7	2.3	115.2
	9	3	16.8	44.0		6	6	13.1	106.1
	10	2	23.8	30.9		7	5	24.3	97.2
	11	1	28.4	16.0		8	4	35.8	87.8
	12		30.0	0.0		9	3	47.2	76.7
February 21	7	5	4.8	72.7	August 21	10	2	57.9	61.7
	8	4	15.4	62.2		11	1	66.7	37.9
	9	3	25.0	50.2		12		70.6	0.0
	10	2	32.8	35.9		6	6	7.9	99.5
	11	1	38.1	18.9		7	5	19.3	90.9
March 21	12		40.0	0.0	September 21	8	4	30.7	79.9
	7	5	11.4	80.2		9	3	41.8	67.9
	8	4	22.5	69.6		10	2	51.7	52.1
	9	3	32.8	57.3		11	1	59.3	29.7
	10	2	41.6	41.9		12		62.3	0.0
April 21	11	1	47.7	22.6	October 21	7	5	11.4	80.2
	12		50.0	0.0		8	4	22.5	69.6
	6	6	7.4	98.9		9	3	32.8	57.3
	7	5	18.9	89.5		10	2	41.6	41.9
	8	4	30.3	79.3		11	1	47.7	22.6
May 21	9	3	41.3	67.2	November 21	12		50.0	0.0
	10	2	51.2	51.4		7	5	4.5	72.3
	11	1	58.7	29.2		8	4	15.0	61.9
	12		61.6	0.0		9	3	24.5	49.8
	5	7	1.9	114.7		10	2	32.4	35.6
June 21	6	6	12.7	105.6	December 21	11	1	37.6	18.7
	7	5	24.0	96.6		12		39.5	0.0
	8	4	35.4	87.2		8	4	8.2	55.4
	9	3	46.8	76.0		9	3	17.0	44.1
	10	2	57.5	60.9		10	2	24.0	31.0
	11	1	66.2	37.1		11	1	28.6	16.1
	12		70.0	0.0		12		30.2	0.0
	5	7	4.2	117.3		8	4	5.5	53.0
	6	6	14.8	108.4		9	3	14.0	41.9
	7	5	26.0	99.7		10	2	20.0	29.4
	8	4	37.4	90.7		11	1	25.0	15.2
	9	3	48.8	80.2		12		26.6	0.0
	10	2	59.8	65.8					
	11	1	69.2	41.9					
	12		73.5	0.0					

in which a_w is the "wall" azimuth angle and β is the surface tilt angle relative to the horizontal plane, both as shown in Fig. 49.5.

For fixed surfaces that face due south, the incidence angle expression simplifies to

$$\cos i = \sin(L - \beta)\sin \delta_s + \cos(L - \beta)\cos \delta_s \cos h_s \tag{49.11}$$

A large class of solar collectors move in some fashion to track the sun's diurnal motion, thereby improving the capture of solar energy. This is accomplished by reduced incidence angles for properly tracking surfaces vis-à-vis a fixed surface for which large incidence angles occur in the early morning and late afternoon (for generally equator-facing surfaces). Table 49.2 lists incidence angle expressions for nine different types of tracking surfaces. The term "polar axis" in this table refers to an axis of

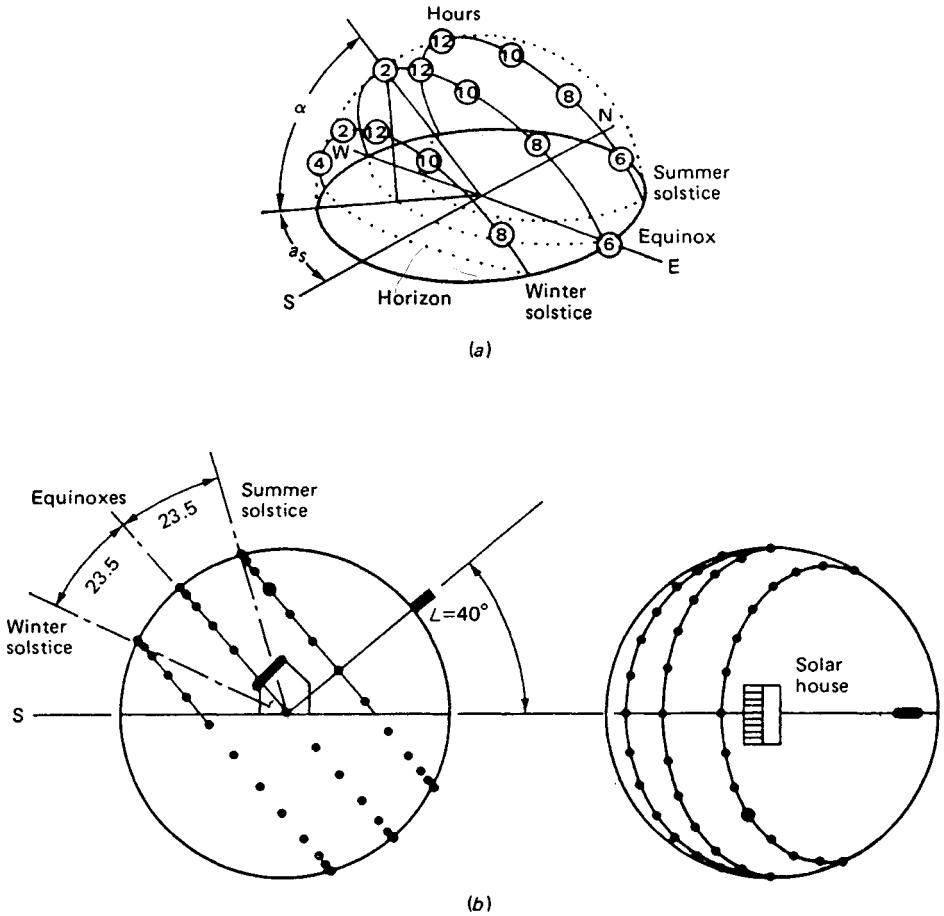


Fig. 49.4 Sun paths for the summer solstice (6/21), the equinoxes (3/21 and 9/21), and the winter solstice (12/21) for a site at 40°N ; (a) isometric view; (b) elevation and plan views.

rotation directed at the north or south pole. This axis of rotation is tilted up from the horizontal at an angle equal to the local latitude. It is seen that normal incidence can be achieved (i.e., $\cos i = 1$) for any tracking scheme for which two axes of rotation are present. The polar case has relatively small incidence angles as well, limited by the declination to $\pm 23.45^\circ$. The mean value of $\cos i$ for polar tracking is 0.95 over a year, nearly as good as the two-axis case for which the annual mean value is unity.

49.1.3 Quantitative Solar Flux Availability

The previous section has indicated how variations in solar flux produced by seasonal and diurnal effects can be quantified. However, the effect of weather on solar energy availability cannot be analyzed theoretically; it is necessary to rely on historical weather reports and empirical correlations for calculations of actual solar flux. In this section this subject is described along with the availability of solar energy at the edge of the atmosphere—a useful correlating parameter, as seen shortly.

Extraterrestrial Solar Flux

The flux intensity at the edge of the atmosphere can be calculated strictly from geometric considerations if the direct-normal intensity is known. Solar flux incident on a terrestrial surface, which has traveled from sun to earth with negligible change in direction, is called beam radiation and is denoted by I_b . The extraterrestrial value of I_b averaged over a year is called the solar constant, denoted by I_{sc} . Its value is $429 \text{ Btu/hr} \cdot \text{ft}^2$ or 1353 W/m^2 . Owing to the eccentricity of the earth's orbit, however, the extraterrestrial beam radiation intensity varies from this mean solar constant value. The variation of I_b over the year is given by

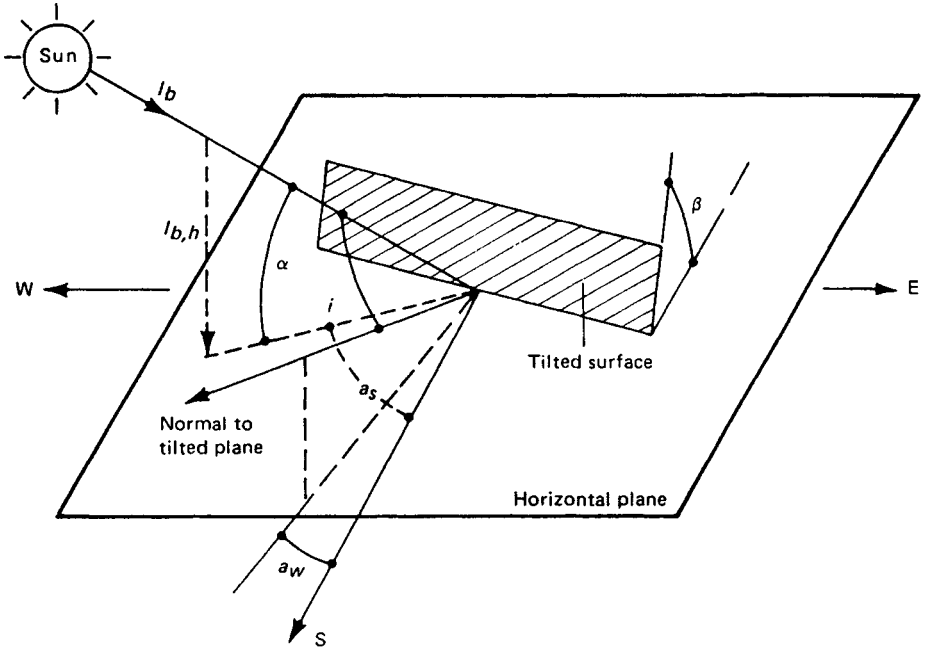


Fig. 49.5 Definition of incidence angle i , surface tilt angle β , solar-altitude angle α , wall-azimuth angle a_w , and solar-azimuth angle a_s for a non-south-facing tilted surface. Also shown is the beam component of solar radiation I_b and the component of beam radiation $I_{b,h}$ on a horizontal plane.

$$I_{b,0}(N) = \left[1 + 0.034 \cos \left(\frac{360 N}{265} \right) \right] \times I_{sc} \tag{49.12}$$

in which N is the day number as before.

In subsequent sections the total daily, extraterrestrial flux will be particularly useful as a nondimensionalizing parameter for terrestrial solar flux data. The instantaneous solar flux on a horizontal, extraterrestrial surface is given by

$$I_{b,h0} = I_{b,0}(N) \sin \alpha \tag{49.13}$$

as shown in Fig. 49.5. The daily total, horizontal radiation is denoted by I_0 and is given by

$$I_0(N) = \int_{t_{sr}}^{t_{ss}} I_{b,0}(N) \sin \alpha dt \tag{49.14}$$

$$I_0(N) = \frac{24}{\pi} I_{sc} \left[1 + 0.034 \cos \left(\frac{360 N}{265} \right) \right] \times (\cos L \cos \delta_s \sin h_{sr} + h_{sr} \sin L \sin \delta_s) \tag{49.15}$$

in which I_{sc} is the solar constant. The extraterrestrial flux varies with time of year via the variations of δ_s and h_{sr} with time of year. Table 49.3 lists the values of extraterrestrial, horizontal flux for various latitudes averaged over each month. The monthly averaged, horizontal, extraterrestrial solar flux is denoted by \bar{H}_0 .

Terrestrial Solar Flux

Values of instantaneous or average terrestrial solar flux cannot be predicted accurately owing to the complexity of atmospheric processes that alter solar flux magnitudes and directions relative to their extraterrestrial values. Air pollution, clouds of many types, precipitation, and humidity all affect the values of solar flux incident on earth. Rather than attempting to predict solar availability accounting for these complex effects, one uses long-term historical records of terrestrial solar flux for design purposes.

Table 49.2 Solar Incidence Angle Equations for Tracking Collectors

Description	Axis (Axes)	Cosine of Incidence Angle ($\cos i$)
Movements in altitude and azimuth	Horizontal axis and vertical axis	1
Rotation about a polar axis and adjustment in declination	Polar axis and declination axis	1
Uniform rotation about a polar axis	Polar axis	$\cos \delta_s$
East–west horizontal	Horizontal, east–west axis	$\sqrt{1 - \cos^2 \alpha \sin^2 a_s}$
North–south horizontal	Horizontal, north–south axis	$\sqrt{1 - \cos^2 \alpha \cos^2 a_s}$
Rotation about a vertical axis of a surface tilted upward L (latitude) degrees	Vertical axis	$\sin(\alpha + L)$
Rotation of a horizontal collector about a vertical axis	Vertical axis	$\sin \alpha$
Rotation of a vertical surface about a vertical axis	Vertical axis	$\cos \alpha$
Fixed “tubular” collector	North–south tiled up at angle β	$\sqrt{1 - [\sin(\beta - L) \cos \delta_s \cos h_s + \cos(\beta - L) \sin \delta_s]^2}$

Table 49.3 Average Extraterrestrial Radiation on a Horizontal Surface \bar{H}_0 in SI Units and in English Units Based on a Solar Constant of 429 Btu/hr · ft² or 1.353 kW/m²

Latitude, Degrees	January	February	March	April	May	June	July	August	September	October	November	December
<i>SI Units, W · hr/m² · Day</i>												
20	7415	8397	9552	10,422	10,801	10,868	10,794	10,499	9791	8686	7598	7076
25	6656	7769	9153	10,312	10,936	11,119	10,988	10,484	9494	8129	6871	6284
30	5861	7087	8686	10,127	11,001	11,303	11,114	10,395	9125	7513	6103	5463
35	5039	6359	8153	9869	10,995	11,422	11,172	10,233	8687	6845	5304	4621
40	4200	5591	7559	9540	10,922	11,478	11,165	10,002	8184	6129	4483	3771
45	3355	4791	6909	9145	10,786	11,477	11,099	9705	7620	5373	3648	2925
50	2519	3967	6207	8686	10,594	11,430	10,981	9347	6998	4583	2815	2100
55	1711	3132	5460	8171	10,358	11,352	10,825	8935	6325	3770	1999	1320
60	963	2299	4673	7608	10,097	11,276	10,657	8480	5605	2942	1227	623
65	334	1491	3855	7008	9852	11,279	10,531	8001	4846	2116	544	97
<i>English Units, Btu/ft² · Day</i>												
20	2346	2656	3021	3297	3417	3438	3414	3321	3097	2748	2404	2238
25	2105	2458	2896	3262	3460	3517	3476	3316	3003	2571	2173	1988
30	1854	2242	2748	3204	3480	3576	3516	3288	2887	2377	1931	1728
35	1594	2012	2579	3122	3478	3613	3534	3237	2748	2165	1678	1462
40	1329	1769	2391	3018	3455	3631	3532	3164	2589	1939	1418	1193
45	1061	1515	2185	2893	3412	3631	3511	3070	2410	1700	1154	925
50	797	1255	1963	2748	3351	3616	3474	2957	2214	1450	890	664
55	541	991	1727	2585	3277	3591	3424	2826	2001	1192	632	417
60	305	727	1478	2407	3194	3567	3371	2683	1773	931	388	197
65	106	472	1219	2217	3116	3568	3331	2531	1533	670	172	31

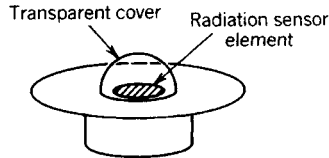
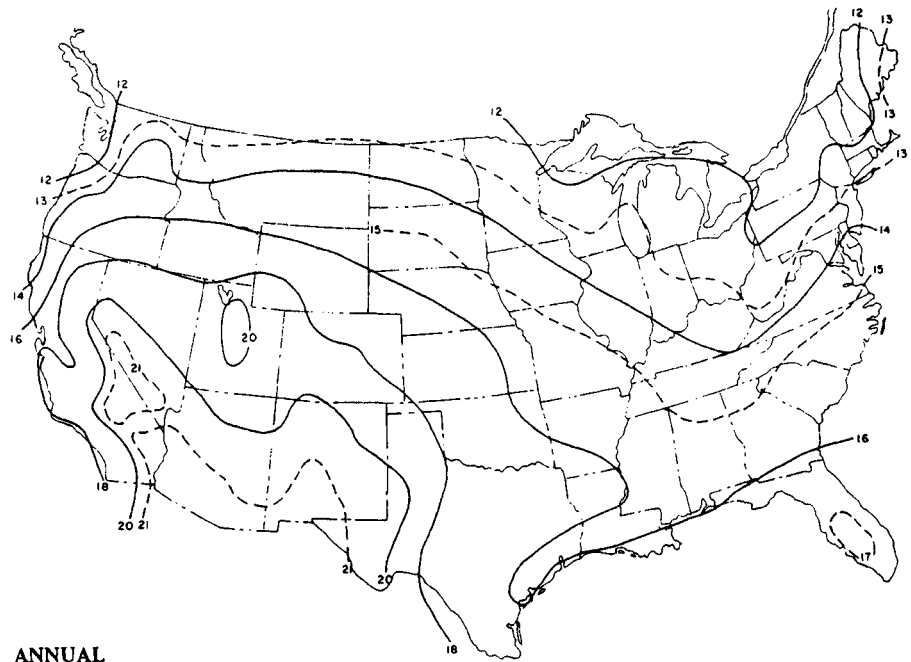


Fig. 49.6 Schematic drawing of a pyranometer used for measuring the intensity of total (direct plus diffuse) solar radiation.

The U.S. National Weather Service (NWS) records solar flux data at a network of stations in the United States. The pyranometer instrument, as shown in Fig. 49.6, is used to measure the intensity of horizontal flux. Various data sets are available from the National Climatic Center (NCC) of the NWS. Prior to 1975, the solar network was not well maintained; therefore, the pre-1975 data were rehabilitated in the late 1970s and are now available from the NCC on magnetic media. Also, for the period 1950–1975, synthetic solar data have been generated for approximately 250 U.S. sites where solar flux data were not recorded. The predictive scheme used is based on other widely available meteorological data. Finally, since 1977 the NWS has recorded hourly solar flux data at a 38-station network with improved instrument maintenance. In addition to horizontal flux, direct-normal data are recorded and archived at the NCC. Figure 49.7 is a contour map of annual, horizontal flux for the United States based on recent data. The appendix to this chapter contains tabulations of average, monthly solar flux data for approximately 250 U.S. sites.

The principal difficulty with using NWS solar data is that they are available for horizontal surfaces only. Solar-collecting surfaces normally face the general direction of the sun and are, therefore, rarely horizontal. It is necessary to convert measured horizontal radiation to radiation on arbitrarily oriented collection surfaces. This is done using empirical approaches to be described.



$$*1 \text{ MJ/m}^2 = 88.1 \text{ Btu/ft}^2.$$

Fig. 49.7 Mean daily solar radiation on a horizontal surface in megajoules per square meter for the continental United States.

Hourly Solar Flux Conversions

Measured, horizontal solar flux consists of both beam and diffuse radiation components. Diffuse radiation is that scattered by atmospheric processes; it intersects surfaces from the entire sky dome, not just from the direction of the sun. Separating the beam and diffuse components of measured, horizontal radiation is the key difficulty in using NWS measurements.

The recommended method for finding the beam component of total (i.e., beam plus diffuse) radiation is described in Ref. 1. It makes use of the parameter k_T called the clearness index and defined as the ratio of terrestrial to extraterrestrial hourly flux on a horizontal surface. In equation form k_T is

$$k_T \equiv \frac{I_h}{I_{b,h0}} = \frac{I_h}{I_{b,0}(N) \sin \alpha} \quad (49.16)$$

in which I_h is the measured, total horizontal flux. The beam component of the terrestrial flux is then given by the empirical equation

$$I_b = (ak_T + b)I_{b,0}(N) \quad (49.17)$$

in which the empirical constants a and b are given in Table 49.4. Having found the beam radiation, the horizontal diffuse component $I_{d,h}$ is found by the simple difference

$$I_{d,h} = I_h - I_b \sin \alpha \quad (49.18)$$

The separate values of horizontal beam and diffuse radiation can be used to find radiation on any surface by applying appropriate geometric "tilt factors" to each component and forming the sum accounting for any radiation reflected from the foreground. The beam radiation incident on any surface is simply $I_b \cos i$. If one assumes that the diffuse component is isotropically distributed over the sky dome, the amount intercepted by any surface tilted at an angle β is $I_{d,h} \cos^2(\beta/2)$. The total beam and diffuse radiation intercepted by a surface I_c is then

$$I_c = I_b \cos i + I_{d,h} \cos^2(\beta/2) + \rho I_h \sin^2(\beta/2) \quad (49.19)$$

The third term in this expression accounts for flux reflected from the foreground with reflectance ρ .¹

Monthly Averaged, Daily Solar Flux Conversions

Most performance prediction methods make use of monthly averaged solar flux values. Horizontal flux data are readily available (see the appendix), but monthly values on arbitrarily positioned surfaces must be calculated using a method similar to that previously described for hourly tilted surface calculations. The monthly averaged flux on a tilted surface \bar{I}_c is given by

$$\bar{I}_c = \bar{R} \bar{H}_h \quad (49.20)$$

in which \bar{H}_h is the monthly averaged, daily total of horizontal solar flux and \bar{R} is the overall tilt factor given by Eq. (49.21) for a fixed, equator-facing surface:

Table 49.4 Empirical Coefficients for Eq. (49.17)

Interval for k_T	a	b
0.00, 0.05	0.04	0.00
0.05, 0.15	0.01	0.002
0.15, 0.25	0.06	-0.006
0.25, 0.35	0.32	-0.071
0.35, 0.45	0.82	-0.246
0.45, 0.55	1.56	-0.579
0.55, 0.65	1.69	-0.651
0.65, 0.75	1.49	-0.521
0.75, 0.85	0.27	0.395

$$\bar{R} = \left(1 - \frac{\bar{D}_h}{\bar{H}_h}\right) \bar{R}_b + \frac{\bar{D}_h}{\bar{H}_h} \cos^2 \frac{\beta}{2} + \rho \sin^2 \frac{\beta}{2} \quad (49.21)$$

The ratio of monthly averaged diffuse to total flux, \bar{D}_h/\bar{H}_h is given by

$$\frac{\bar{D}_h}{\bar{H}_h} = 0.775 + 0.347 \left[h_{sr} - \frac{\pi}{2} \right] - \left[0.505 + 0.261 \left(h_{sr} - \frac{\pi}{2} \right) \right] \cos \left[(\bar{K}_T - 0.9) \frac{360}{\pi} \right] \quad (49.22)$$

in which \bar{K}_T is the monthly averaged clearness index analogous to the hourly clearness index. \bar{K}_T is given by

$$\bar{K}_T = \bar{H}_h/\bar{H}_0$$

where H_0 is the monthly averaged, extraterrestrial radiation on a horizontal surface at the same latitude at which the terrestrial radiation \bar{H}_h was recorded. The monthly averaged beam radiation tilt factor \bar{R}_b is

$$\bar{R}_b = \frac{\cos(L - \beta) \cos \delta_s \sin h'_{sr} + h'_{sr} \sin(L - \beta) \sin \delta_s}{\cos L \cos \delta_s \sin h_{sr} + h_{sr} \sin L \sin \delta_s} \quad (49.23)$$

The sunrise hour angle is found from Eq. (49.9) and the value of h'_{sr} is the smaller of (1) the sunrise hour angle h_{sr} and (2) the collection surface sunrise hour angle found by setting $i = 90^\circ$ in Eq. (49.11). That is, h'_{sr} is given by

$$h'_{sr} = \min\{\cos^{-1}[-\tan L \tan \delta_s], \cos^{-1}[-\tan(L - \beta) \tan \delta_s]\} \quad (49.24)$$

Expressions for solar flux on a tracking surface on a monthly averaged basis are of the form

$$\bar{I}_c = \left[r_T - r_d \left(\frac{\bar{D}_h}{\bar{H}_h} \right) \right] \bar{H}_h \quad (49.25)$$

in which the tilt factors r_T and r_d are given in Table 49.5. Equation (49.22) is to be used for the diffuse to total flux ratio \bar{D}_h/\bar{H}_h .

49.2 SOLAR THERMAL COLLECTORS

The principal use of solar energy is in the production of heat at a wide range of temperatures matched to a specific task to be performed. The temperature at which heat can be produced from solar radiation is limited to about 6000°F by thermodynamic, optical, and manufacturing constraints. Between temperatures near ambient and this upper limit very many thermal collector designs are employed to produce heat at a specified temperature. This section describes the common thermal collectors.

49.2.1 Flat-Plate Collectors

From a production volume standpoint, the majority of installed solar collectors are of the flat-plate design; these collectors are capable of producing heat at temperatures up to 100°C. Flat-plate collectors are so named since all components are planar. Figure 49.8a is a partial isometric sketch of a liquid-cooled flat-plate collector. From the top down it contains a glazing system—normally one pane of glass, a dark colored metal absorbing plate, insulation to the rear of the absorber, and, finally, a metal or plastic weatherproof housing. The glazing system is sealed to the housing to prohibit the ingress of water, moisture, and dust. The piping shown is thermally bonded to the absorber plate and contains the working fluid by which the heat produced is transferred to its end use. The pipes shown are manifolded together so that one inlet and one outlet connection, only, are present. Figure 49.8b shows a number of other collector designs in common use.

The energy produced by flat-plate collectors is the difference between the solar flux absorbed by the absorber plate and that lost from it by convection and radiation from the upper (or “front”) surface and that lost by conduction from the lower (or “back”) surface. The solar flux absorbed is the incident flux I_c multiplied by the glazing system transmittance τ and by the absorber plate absorptance α . The heat lost from the absorber in steady state is given by an overall thermal conductance U_c multiplied by the difference in temperature between the collector absorber temperature T_c and the surrounding, ambient temperature T_a . In equation form the net heat produced q_u is then

$$q_u = (\tau\alpha)I_c - U_c(T_c - T_a) \quad (49.26)$$

The rate of heat production depends on two classes of parameters. The first— T_c , T_a , and I_c —having

Table 49.5 Concentrator Tilt Factors

Collector Type	$r_T^{a,b,c,d}$	r_d^e
Fixed aperture concentrators that do not view the foreground	$\begin{aligned} & [\cos(L - \beta)/(d \cos L)]\{-ah_{\text{coll}} \cos h_{sr}(i = 90^\circ) \\ & + [a - b \cos h_{sr}(i = 90^\circ)] \sin h_{\text{coll}} \\ & + (b/2)(\sin h_{\text{coll}} \cos h_{\text{coll}} + h_{\text{coll}})\} \end{aligned}$	$\begin{aligned} & (\sin h_{\text{coll}}/d)\{[\cos(L + \beta)/\cos L] - [1/(\text{CR})]\} + (h_{\text{coll}}/d)\{[\cos h_{sr}/(\text{CR})] \\ & - [\cos(L - \beta)/\cos L] \cos h_{sr}(i = 90^\circ)\} \end{aligned}$
East-west axis tracking ^f	$(1/d) \int_0^{h_{\text{coll}}} \{(a + b \cos x)/\cos L\} \times \sqrt{\cos^2 x + \tan^2 \delta_s} dx$	$(1/d) \int_0^{h_{\text{coll}}} \{(1/\cos L)\sqrt{\cos^2 x + \tan^2 \delta_s} - [1/(\text{CR})][\cos x - \cos h_{sr}]\} dx$
Polar tracking	$(ah_{\text{coll}} + b \sin h_{\text{coll}})/(d \cos L)$	$(h_{\text{coll}}/d)\{(1/\cos L) + [\cos h_{sr}/(\text{CR})]\} - \sin h_{\text{coll}}/[d(\text{CR})]$
Two-axis tracking	$(ah_{\text{coll}} + b \sin h_{\text{coll}})/(d \cos \delta_s \cos L)$	$(h_{\text{coll}}/d)[1/\cos \delta_s \cos L] + [\cos h_{sr}/(\text{CR})] - h_{\text{coll}}/[d(\text{CR})]$

^aThe collection hour angle value h_{coll} not used as the argument of trigonometric functions is expressed in radians; note that the total collection interval, $2h_{\text{coll}}$, is assumed to be centered about solar noon.

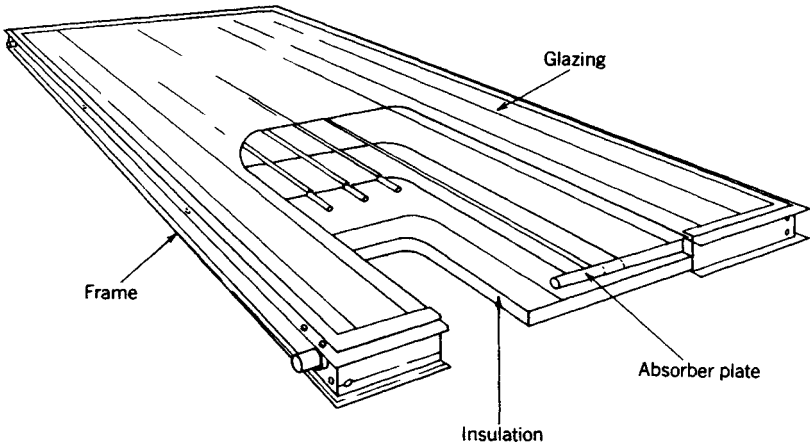
^b $a = 0.409 + 0.5016 \sin(h_{sr} - 60^\circ)$.

^c $c = 0.6609 - 0.4767 \sin(h_{sr} - 60^\circ)$.

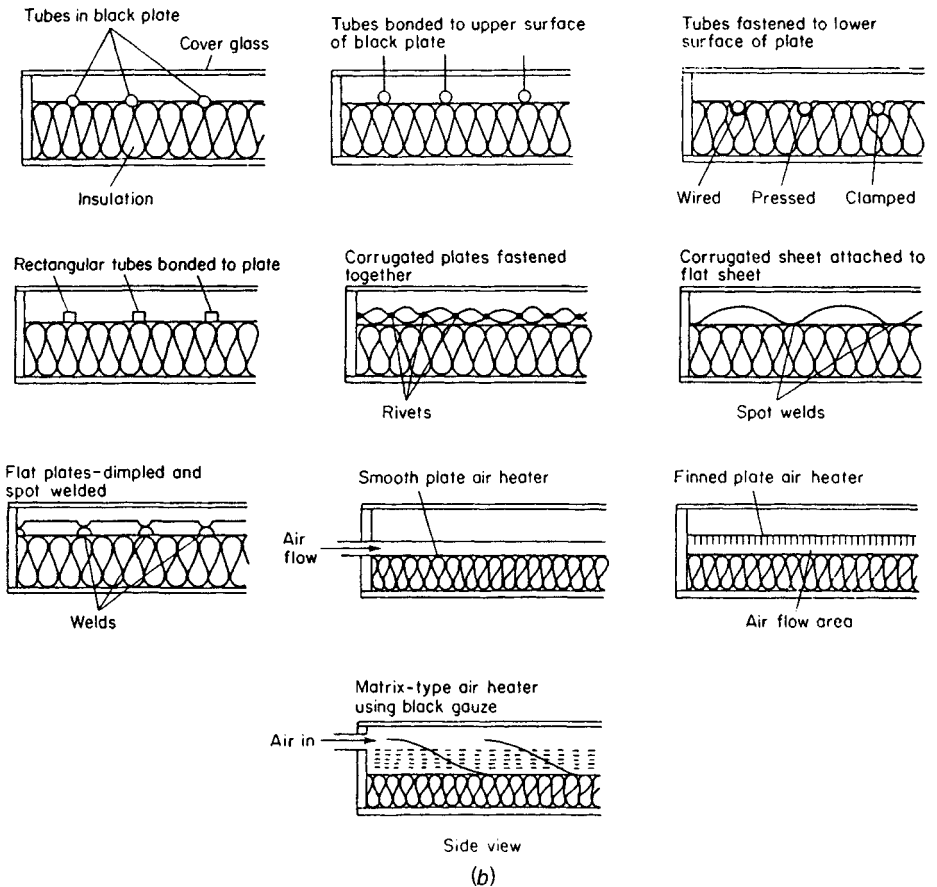
^d $d = \sin h_{sr} - h_{sr} \cos h_{sr}; \cos h_{sr}(i = 90^\circ) = -\tan \delta_s \tan(L - \beta)$.

^eCR is the collector concentration ratio.

^fUse elliptic integral tables to evaluate terms of the form of $\int_0^h \sqrt{\cos^2 x + \tan^2 \delta_s} dx$ contained in r_T and r_d .



(a)



(b)

Fig. 49.8 (a) Schematic diagram of solar collector with one cover. (b) Cross sections of various liquid- and air-based flat-plate collectors in common use.

to do with the operational environment and the condition of the collector. The second— U_c and $\tau\alpha$ —are characteristics of the collector independent of where or how it is used. The optical properties τ and α depend on the incidence angle, both dropping rapidly in value for $i > 50\text{--}55^\circ$. The heat loss conductance can be calculated,^{1,2} but formal tests, as subsequently described, are preferred for the determination of both $\tau\alpha$ and U_c .

Collector efficiency is defined as the ratio of heat produced q_u to incident flux I_c , that is,

$$\eta_c \equiv q_u / I_c \tag{49.27}$$

Using this definition with Eq. (49.26) gives the efficiency as

$$\eta_c = \tau\alpha - U_c \left(\frac{T_c - T_a}{I_c} \right) \tag{49.28}$$

The collector plate temperature is difficult to measure in practice, but the fluid inlet temperature $T_{f,i}$ is relatively easy to measure. Furthermore, $T_{f,i}$ is often known from characteristics of the process to which the collector is connected. It is common practice to express the efficiency in terms of $T_{f,i}$ instead of T_c for this reason. The efficiency is

$$\eta_c = F_R \left[\tau\alpha - U_c \left(\frac{T_{f,i} - T_a}{I_c} \right) \right] \tag{49.29}$$

in which the heat removal factor F_R is introduced to account for the use of $T_{f,i}$ for the efficiency basis. F_R depends on the absorber plate thermal characteristics and heat loss conductance.²

Equation (49.29) can be plotted with the group of operational characteristics $(T_{f,i} - T_a)/I_c$ as the independent variable as shown in Fig. 49.9. The efficiency decreases linearly with the abscissa value. The intercept of the efficiency curve is the optical efficiency $\tau\alpha$ and the slope is $-F_R U_c$. Since the glazing transmittance and absorber absorptance decrease with solar incidence angle, the efficiency

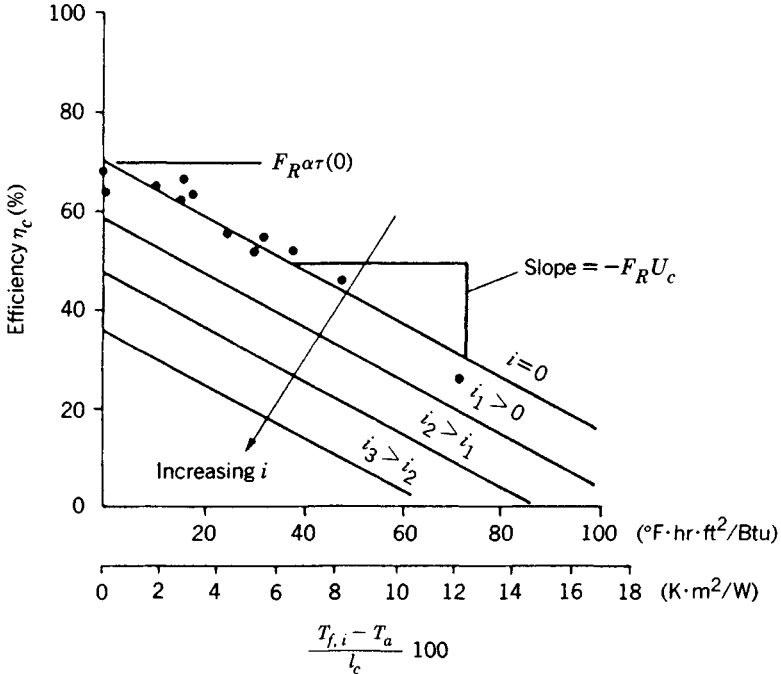


Fig. 49.9 Typical collector performance with 0° incident beam flux angle. Also shown qualitatively is the effect of incidence angle i , which may be quantified by $\bar{\tau}\alpha(i)/\bar{\tau}\alpha(0) = 1.0 + b_0(1/\cos i - 1.0)$, where b_0 is the incidence angle modifier determined experimentally (ASHRAE 93-77) or from the Stokes and Fresnel equations.

curve migrates toward the origin with increasing incidence angle, as shown in the figure. Data points from a collector test are also shown on the plot. The best-fit efficiency curve at normal incidence ($i = 0$) is determined numerically by a curve-fit method. The slope and intercept of the experimental curve, so determined, are the preferred values of the collector parameters as opposed to those calculated theoretically.

Selective Surfaces

One method of improving efficiency is to reduce radiative heat loss from the absorber surface. This is commonly done by using a low emittance (in the infrared region) surface having high absorptance for solar flux. Such surfaces are called (wavelength) selective surface and are used on very many flat-plate collectors to improve efficiency at elevated temperature. Table 49.6 lists emittance and absorptance values for a number of common selective surfaces. Black chrome is very reliable and cost effective.

49.2.2 Concentrating Collectors

Another method of improving the efficiency of solar collectors is to reduce the parasitic heat loss embodied in the second term of Eq. (49.29). This can be done by reducing the size of the absorber relative to the aperture area. Relatively speaking, the area from which heat is lost is smaller than the heat collection area and efficiency increases. Collectors that focus sunlight onto a relatively small absorber can achieve excellent efficiency at temperatures above which flat-plate collectors produce no net heat output. In this section a number of concentrators are described.

Trough Collectors

Figure 49.10 shows cross sections of five concentrators used for producing heat at temperatures up to 650°F at good efficiency. Figure 49.10a shows the parabolic "trough" collector representing the most common concentrator design available commercially. Sunlight is focused onto a circular pipe absorber located along the focal line. The trough rotates about the absorber centerline in order to maintain a sharp focus of incident beam radiation on the absorber. Selective surfaces and glass enclosures are used to minimize heat losses from the absorber tube.

Figures 49.10c and 49.10d show Fresnel-type concentrators in which the large reflector surface is subdivided into several smaller, more easily fabricated and shipped segments. The smaller reflector elements are easier to track and offer less wind resistance at windy sites; furthermore, the smaller reflectors are less costly. Figure 49.10e shows a Fresnel lens concentrator. No reflection is used with this approach; reflection is replaced by refraction to achieve the focusing effect. This device has the advantage that optical precision requirements can be relaxed somewhat relative to reflective methods.

Figure 49.10b shows schematically a concentrating method in which the mirror is fixed, thereby avoiding all problems associated with moving large mirrors to track the sun as in the case of concentrators described above. Only the absorber pipe is required to move to maintain a focus on the focal line.

The useful heat produced Q_u by any concentrator is given by

$$Q_u = A_a \eta_0 I_c - A_r U'_c (T_c - T_a) \quad (49.30)$$

in which the concentrator optical efficiency (analogous to $\tau\alpha$ for flat-plate collectors) is η_0 , the aperture area is A_p , the receiver or absorber area is A_r , and the absorber heat loss conductance is U'_c . Collector efficiency can be found from Eq. (49.27) and is given by

$$\eta_c = \eta_0 - \frac{A_r}{A_a} U'_c \left(\frac{T_c - T_a}{I_c} \right) \quad (49.31a)$$

Table 49.6 Selective Surface Properties

Material	Absorptance ^a α	Emittance ϵ	Comments
Black chrome	0.87–0.93	0.1	
Black zinc	0.9	0.1	
Copper oxide over aluminum	0.93	0.11	
Black copper over copper	0.85–0.90	0.08–0.12	Patinaes with moisture
Black chrome over nickel	0.92–0.94	0.07–0.12	Stable at high temperatures
Black nickel over nickel	0.93	0.06	May be influenced by moisture
Black iron over steel	0.90	0.10	

^aDependent on thickness.

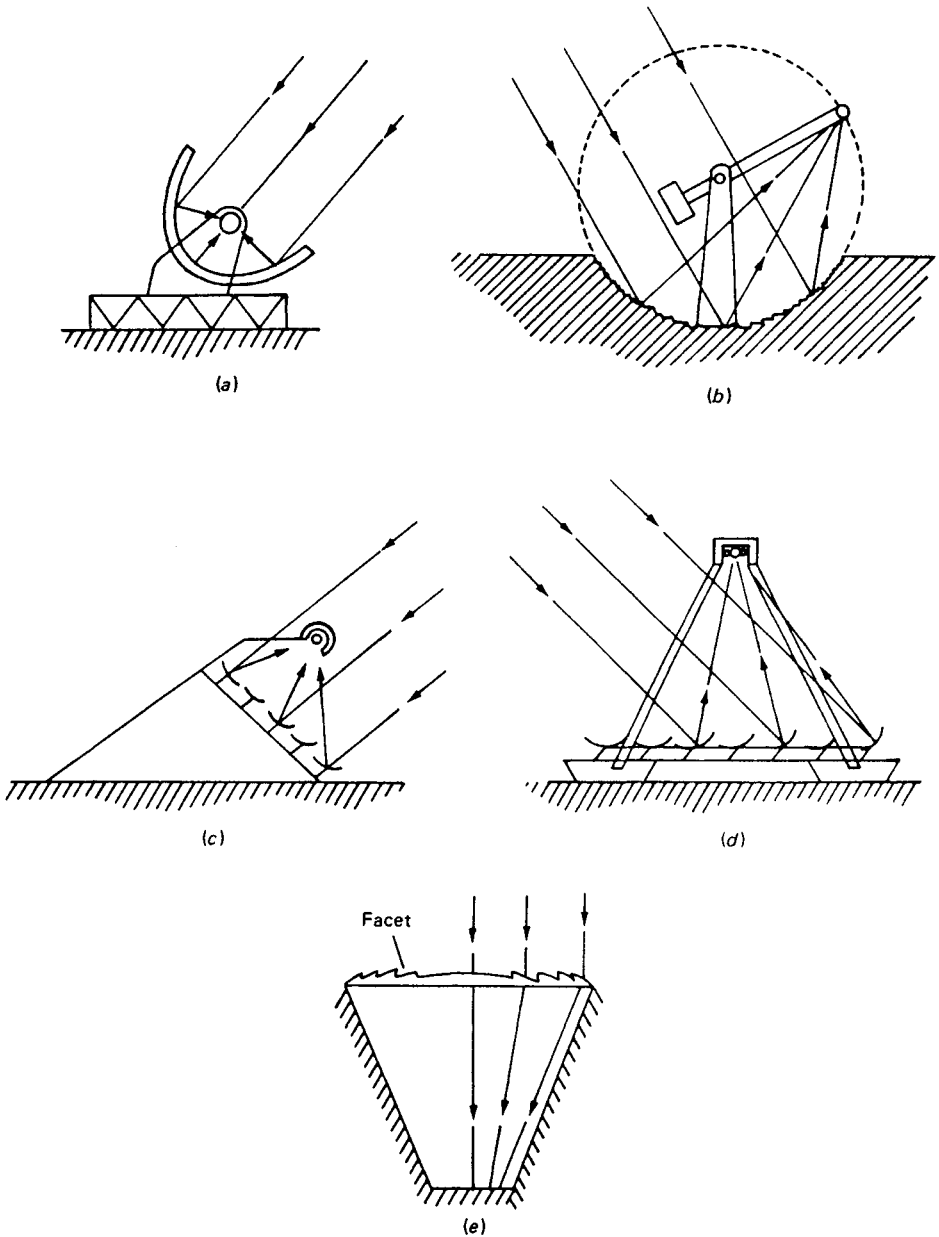


Fig. 49.10 Single-curvature solar concentrators: (a) parabolic trough; (b) fixed circular trough with tracking absorber; (c) and (d) Fresnel mirror designs; and (e) Fresnel lens.

The aperture area-receiver area ratio $A_a/A_r > 1$ is called the geometric concentration ratio CR . It is the factor by which absorber heat losses are reduced relative to the aperture area:

$$\eta_c = \eta_0 - \frac{U'_c}{CR} \left(\frac{T_c - T_a}{I_c} \right) \tag{49.31b}$$

As with flat-plate collectors, efficiency is most often based on collector fluid inlet temperature $T_{f,i}$. On this basis, efficiency is expressed as

$$\eta_c = F_R \left[\eta_0 - U_c \left(\frac{T_{f,i} - T_a}{I_c} \right) \right] \quad (49.32)$$

in which the heat loss conductance U_c on an aperture area basis is used ($U_c = U_c'/CR$).

The optical efficiency of concentrators must account for a number of factors not present in flat-plate collectors including mirror reflectance, shading of aperture by receiver and its supports, spillage of flux beyond receiver tube ends at off-normal incidence conditions, and random surface, tracking, and construction errors that affect the precision of focus. In equation form the general optical efficiency is given by

$$\eta_0 = \rho_m \tau_c \alpha_r f_i \delta F(i) \quad (49.33)$$

where ρ_m is the mirror reflectance (0.8–0.9), τ_c is the receiver cover transmittance (0.85–0.92), α_r is the receiver surface absorptance (0.9–0.92), f_i is the fraction of aperture area not shaded by receiver and its supports (0.95–0.97), δ is the intercept factor accounting for mirror surface and tracking errors (0.90–0.95), and $F(i)$ is the fraction of reflected solar flux intercepted by the receiver for perfect optics and perfect tracking. Values for these parameters are given in Refs. 2 and 4.

Compound Curvature Concentrators

Further increases in concentration and concomitant reductions in heat loss are achievable if “dish-type” concentrators are used. This family of concentrators is exemplified by the paraboloidal dish concentrator, which focuses solar flux at a point instead of along a line as with trough collectors. As a result the achievable concentration ratios are approximately the square of what can be realized with single curvature, trough collectors. Figures 49.11 and 49.12 show a paraboloidal dish concentrator assembly. These devices are of most interest for power production and some elevated industrial process heat applications.

For very large aperture areas it is impractical to construct paraboloidal dishes consisting of a single reflector. Instead the mirror is segmented as shown in Fig. 49.13. This collector system called the central receiver has been used in several solar thermal power plants in the 1–15 MW range. This power production method is discussed in the next section.

The efficiency of compound curvature dish collectors is given by Eq. (49.32), where the parameters involved are defined in the context of compound curvature optics.⁴ The heat loss term at high temperatures achieved by dish concentrators is dominated by radiation; therefore, the second term of the efficiency equation is represented as

$$\eta_c = \eta_0 - \frac{\epsilon_r \sigma (T_c^4 - T_a^4)}{CR} \quad (49.34)$$

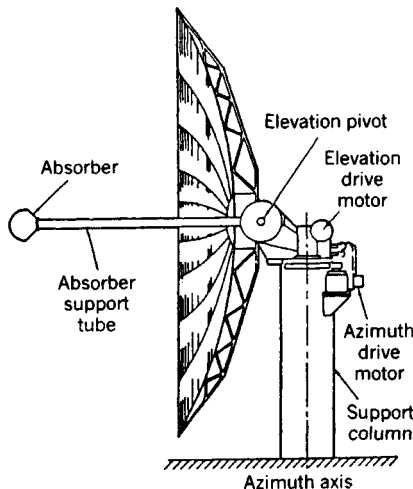


Fig. 49.11 Segmented mirror approximation to paraboloidal dish designed by Raytheon, Inc. Paraboloid is approximated by about 200 spherical mirrors. Average CR is 118, while maximum local CR is 350.



Fig. 49.12 Commercial paraboloidal solar concentrator. The receiver assembly has been removed from the focal zone for this photograph. (Courtesy of Omnium-G Corp., Anaheim, CA.)

where ϵ , the infrared emittance of the receiver, σ is the Stefan-Boltzmann constant, and T'_a is the equivalent ambient temperature for radiation depending on ambient humidity and cloud cover. For clear, dry conditions T'_a is about 15–20°F below the ambient dry bulb temperature. As humidity decreases, T_a approaches the dry bulb temperature.

The optical efficiency for the central receiver is expressed in somewhat different terms than those used in Eq. (49.33). It is referenced to solar flux on a horizontal surface and therefore includes the geometric tilt factor. For the central receiver, the optical efficiency is given by

$$\eta_0 = \phi \rho_m \alpha_r f \delta \quad (49.35)$$

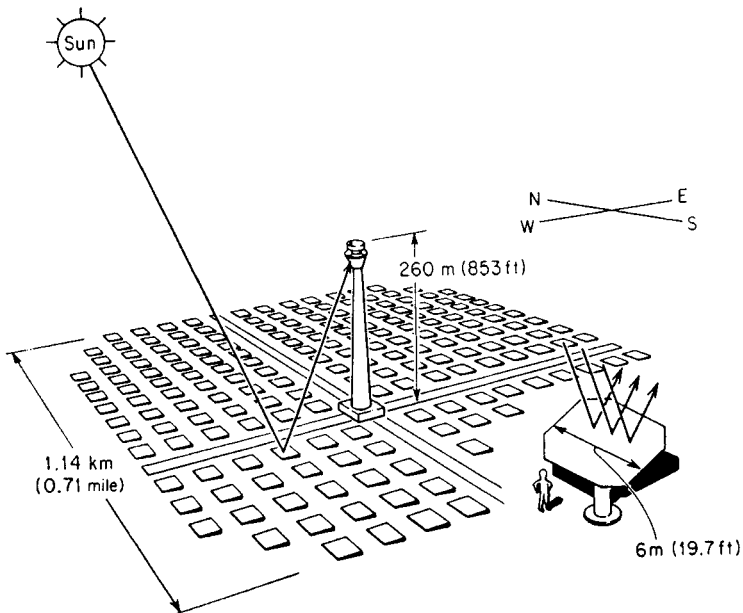


Fig. 49.13 Schematic diagram of a 50-MWe central receiver power plant. A single heliostat is shown in the inset to indicate its human scale. (From Electric Power Research Institute (EPRI).)

in which the last four parameters are defined as in Eq. (49.33). The ratio of redirected flux to horizontal flux is φ and is given approximately by

$$\varphi = 0.78 + 1.5(1 - \alpha/90)^2 \quad (49.36)$$

from Ref. 4. The ratio of mirror area to ground area ϕ depends on the size and economic factors applicable to a specific installation. Values for ϕ have been in the range 0.4–0.5 for installations made through 1985.

49.2.3 Collector Testing

In order to determine the optical efficiency and heat loss characteristics of flat-plate and concentrating collectors (other than the central receiver, which is difficult to test because of its size), testing under controlled conditions is preferred to theoretical calculations. Such test data are required if comparisons among collectors are to be made objectively. As of the mid-1980s very few consensus standards had been adopted by the U.S. solar industry. The ASHRAE Standard Number 93-77 applies to flat-plate collectors that contain either a liquid or a gaseous working fluid.⁵ Collectors in which a phase change occurs are not included. In addition, the standards do not apply well to concentrators, since additional procedures are needed to find the optical efficiency and aging effects. Testing of concentrators uses sections of the above standard where applicable plus additional procedures as needed; however, no industry standard exists. (The ASTM has promulgated standard E905 as the first proposed standard for concentrator tests.) ASHRAE Standard Number 96-80 applies to very-low-temperature collectors manufactured without any glazing system.

Figure 49.14 shows the test loop used for liquid-cooled flat-plate collectors. Tests are conducted with solar flux at near-normal incidence to find the normal incidence optical efficiency $(\tau\alpha)_n$ along with the heat loss conductance U_c . Off-normal optical efficiency is determined in a separate test by orienting the collector such that several substantially off-normal values of $\tau\alpha$ or η_0 can be measured. The fluid used in the test is preferably that to be used in the installed application, although this is not always possible. If operational and test fluids differ, an analytical correction in the heat removal factor F_R is to be made.² An additional test is made after a period of time (nominal one month) to determine the effect of aging, if any, on the collector parameters listed above. A similar test loop and procedure apply to air-cooled collectors.⁵

The development of full system tests has only begun. Of course, it is the entire solar system (see next section) not just the collector that ultimately must be rated in order to compare solar and other

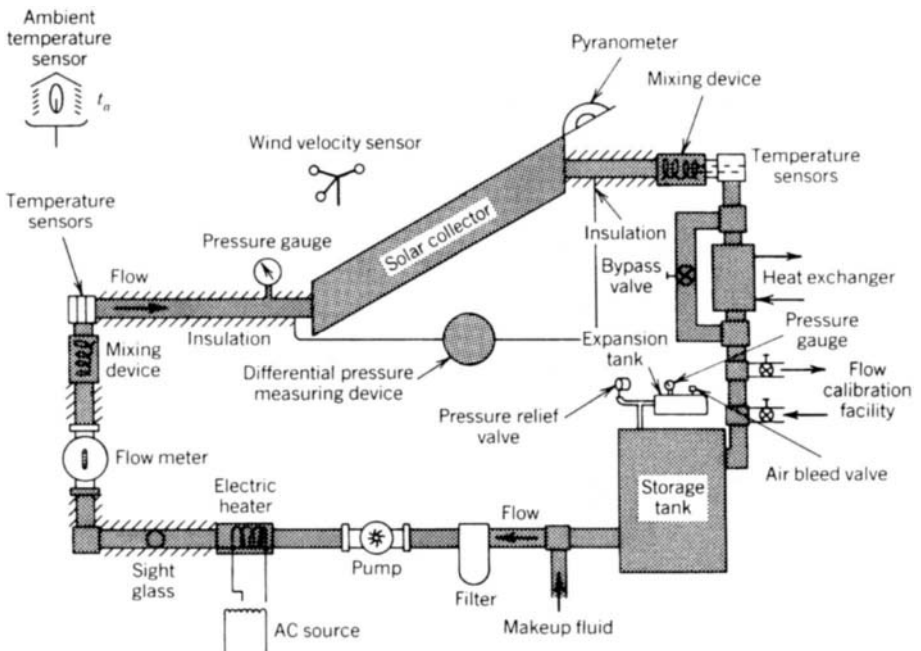


Fig. 49.14 Closed-loop testing configuration for the solar collector when the transfer fluid is a liquid.

energy-conversion systems. Testing of full-size solar systems is very difficult owing to their large size and cost. Hence, it is unlikely that full system tests will ever be practical except for the smallest systems such as residential water heating systems. For this one group of systems a standard test procedure (ASHRAE 95-81) exists. Larger-system performance is often predicted, based on component tests, rather than measured.

49.3 SOLAR THERMAL APPLICATIONS

One of the unique features of solar heat is that it can be produced over a very broad range of temperatures—the specific temperature being selected to match the thermal task to be performed. In this section the most common thermal applications will be described in summary form. These include low-temperature uses such as water and space heating (30–100°C), intermediate temperature industrial processes (100–300°C), and high-temperature thermal power applications (500–850°C and above). Methods for predicting performance, where available, will also be summarized. Nonthermal solar applications are described in the next section.

49.3.1 Solar Water Heating

The most often used solar thermal application is for the heating of water for either domestic or industrial purposes. Relatively simple systems are used, and the load exists relatively uniformly through a year resulting in a good system load factor. Figure 49.15*a* shows a single-tank water heater schematically. The key components are the collector (0.5–1.0 ft²/gal day load), the storage tank (1.0–2.0 gal/ft² of collector), a circulating pump, and controller. The check valve is essential to prevent backflow of collector fluid, which can occur at night when the pump is off if the collectors are located some distance above the storage tank. The controller actuates the pump whenever the collector is 15–30°F warmer than storage. Operation continues until the collector is only 1.5–5°F warmer than the tank, at which point it is no longer worthwhile to operate the pump to collect the relatively small amounts of solar heat available.

The water-heating system shown in Fig. 49.15*a* uses an electrical coil located near the top of the tank to ensure a hot water supply during periods of solar outage. This approach is only useful in small residential systems and where nonsolar energy resources other than electricity are not available. Most commercial systems are arranged as shown in Fig. 49.15*b*, where a separate preheat tank, heated only by solar heat, is connected upstream of the nonsolar, auxiliary water heater tank or plant steam-to-water heat exchanger. This approach is more versatile in that any source of backup energy whatever can be used when solar heat is not available. Additional parasitic heat loss is encountered, since total tank surface area is larger than for the single tank design.

The water-heating systems shown in Fig. 49.15 are of the indirect type, that is, a separate fluid is heated in the collector and heat thus collected is transferred to the end use via a heat exchanger. This approach is needed in locations where freezing occurs in winter and antifreeze solutions are required. The heat exchanger can be eliminated, thereby reducing cost and eliminating the unavoidable fluid temperature decrement between collector and storage fluid streams, if freezing will never occur at the application site. The exchanger can also be eliminated if the “drain-back” approach is used. In this system design the collectors are filled with water only when the circulating pump is on, that is, only when the collectors are warm. If the pump is not operating, the collectors and associated piping all drain back into the storage tank. This approach has the further advantage that heated water otherwise left to cool overnight in the collectors is returned to storage for useful purposes.

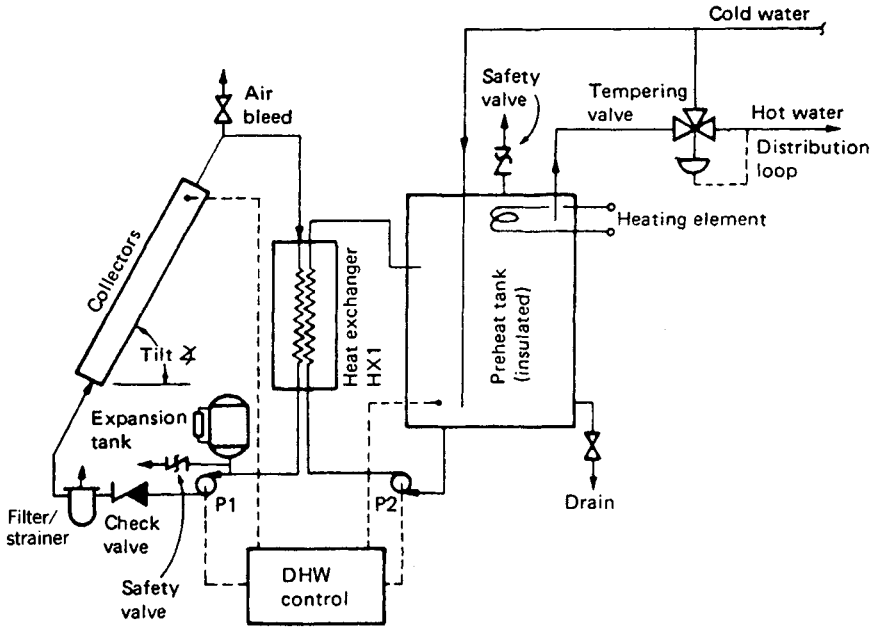
The earliest water heaters did not use circulating pumps, but used the density difference between cold collector inlet water and warmer collector outlet water to produce the flow. This approach is called a “thermosiphon” and is shown in Fig. 49.16. These systems are among the most efficient, since no parasitic use of electric pump power is required. The principal difficulty is the requirement that the large storage tank be located above the collector array, often resulting in structural and architectural difficulties. Few industrial solar water-heating systems have used this approach, owing to difficulties in balancing buoyancy-induced flows in large piping networks.

49.3.2 Mechanical Solar Space Heating Systems

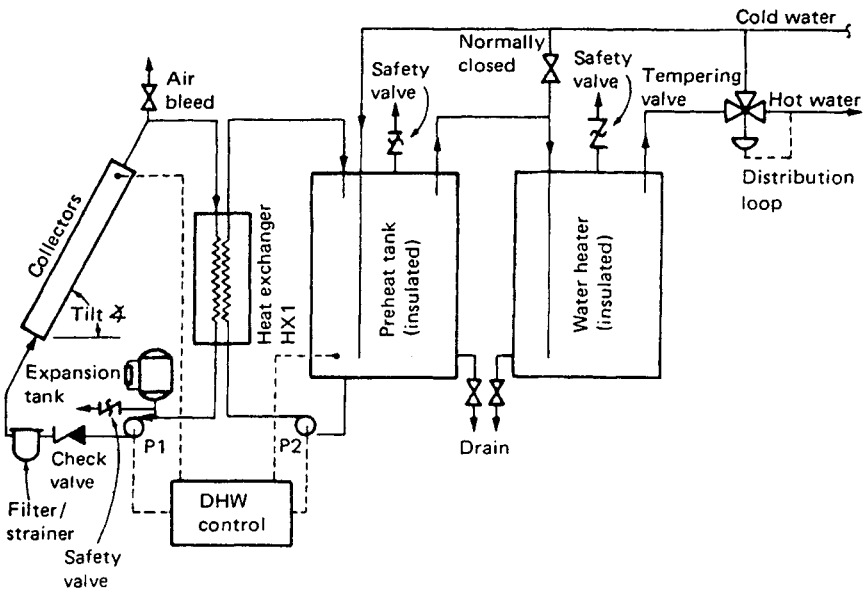
Solar space heating is accomplished using systems similar to those for solar water heating. The collectors, storage tank, pumps, heat exchangers, and other components are larger in proportion to the larger space heat loads to be met by these systems in building applications. Figure 49.17 shows the arrangement of components in one common space heating system. All components except the solar collector and controller have been in use for many years in building systems and are not of special design for the solar application.

The control system is somewhat more complex than that used in nonsolar building heating systems, since two heat sources—solar and nonsolar auxiliary—are to be used under different conditions. Controls using simple microprocessors are available for precise and reliable control of solar space heating systems.

Air-based systems are also widely used for space heating. They are similar to the liquid system shown in Fig. 49.17 except that no heat exchanger is used and rock piles, not tanks of fluid, are the storage media. Rock storage is essential to efficient air-system operation since gravel (usually 1–2



(a)



(b)

Fig. 49.15 (a) Single-tank indirect solar water-heating system. (b) Double-tank indirect solar water-heating system. Instrumentation and miscellaneous fittings are not shown.

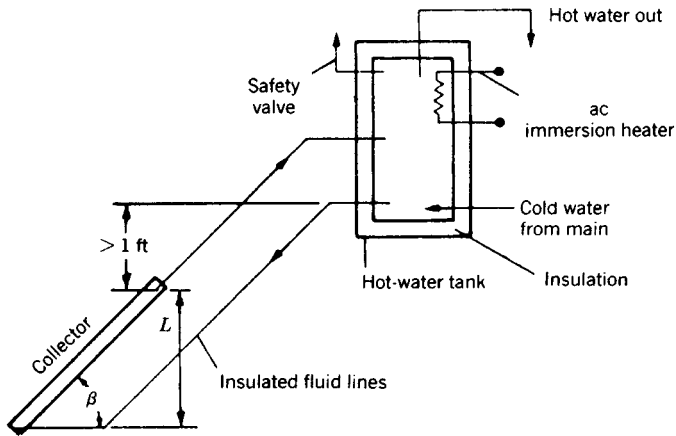


Fig. 49.16 Passive thermosiphon single-tank direct system for solar water heating. Collector is positioned below the tank to avoid reverse circulation.

in. in diameter) has a large surface-to-volume ratio necessary to offset the poor heat transfer characteristics of the air working fluid. Slightly different control systems are used for air-based solar heaters.

49.3.3 Passive Solar Space Heating Systems

A very effective way of heating residences and small commercial buildings with solar energy and without significant nonsolar operating energy is the “passive” heating approach. Solar flux is admitted into the space to be heated by large sun-facing apertures. In order that overheating not occur during sunny periods, large amounts of thermal storage are used, often also serving a structural purpose. A number of classes of passive heating systems have been identified and are described in this section.

Figure 49.18 shows the simplest type of passive system known as “direct gain.” Solar flux enters a large aperture and is converted to heat by absorption on dark colored floors or walls. Heat produced at these wall surfaces is partly conducted into the wall or floor serving as stored heat for later periods without sun. The remaining heat produced at wall or floor surfaces is convected away from the surface thereby heating the space bounded by the surface. Direct-gain systems also admit significant daylight during the day; properly used, this can reduce artificial lighting energy use. In cold climates significant heat loss can occur through the solar aperture during long, cold winter nights. Hence, a necessary component of efficient direct-gain systems is some type of insulation system put in place at night over the passive aperture. This is indicated by the dashed lines in the figure.

The second type of passive system commonly used is variously called the thermal storage wall (TSW) or collector storage wall. This system, shown in Fig. 49.19, uses a storage mass interposed between the aperture and space to be heated. The reason for this positioning is to better illuminate storage for a significant part of the heating season and also to obviate the need for a separate insulation system; selective surfaces applied to the outer storage wall surface are able to control heat loss well in cold climates, while having little effect on solar absorption. As shown in the figure, a thermocirculation loop is used to transport heat from the warm, outer surface of the storage wall to the space interior to the wall. This air flow convects heat into the space during the day, while conduction through the wall heats the space after sunset. Typical storage media include masonry, water, and selected eutectic mixtures of organic and inorganic materials. The storage wall eliminates glare problems associated with direct-gain systems, also.

The third type of passive system in use is the attached greenhouse or “sunspace” as shown in Fig. 49.20. This system combines certain features of both direct-gain and storage wall systems. Night insulation may or may not be used, depending on the temperature control required during nighttime.

The key parameters determining the effectiveness of passive systems are the optical efficiency of the glazing system, the amount of directly illuminated storage and its thermal characteristics, the available solar flux in winter, and the thermal characteristics of the building of which the passive system is a part. In a later section, these parameters will be quantified and will be used to predict the energy saved by the system for a given building in a given location.

49.3.4 Solar Ponds

A “solar pond” is a body of water no deeper than a few meters configured in such a way that usual convection currents induced by solar absorption are suppressed. The oldest method for convection

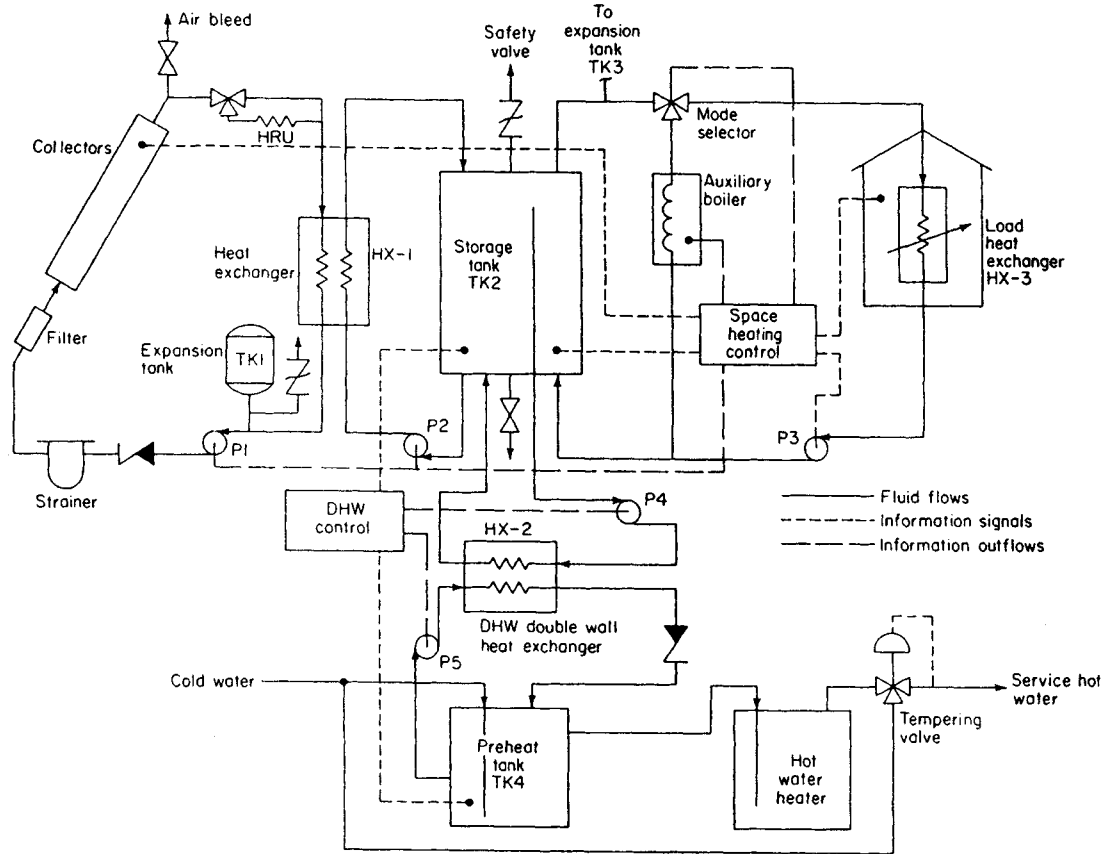


Fig. 49.17 Schematic diagram of a typical liquid-based space heating system with domestic water preheat.

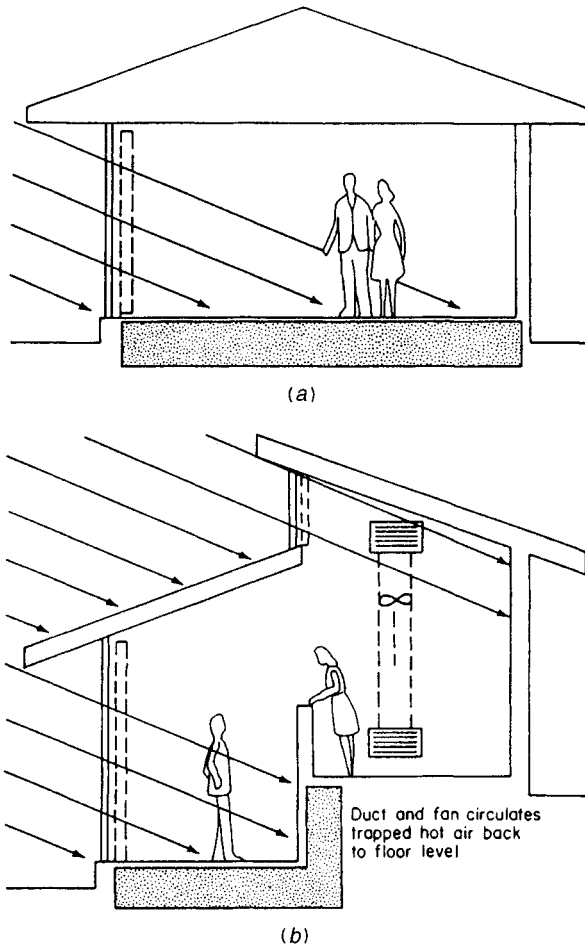


Fig. 49.18 Direct-gain passive heating systems: (a) adjacent space heating; (b) clerestory for north zone heating.

suppression is the use of high concentrations of soluble salts in layers near the bottom of the pond with progressively smaller concentrations near the surface. The surface layer itself is usually fresh water. Incident solar flux is absorbed by three mechanisms. Within a few millimeters of the surface the infrared component (about one-third of the total solar flux energy content) is completely absorbed. Another third is absorbed as the visible and ultraviolet components traverse a pond of nominal 2-m depth. The remaining one-third is absorbed at the bottom of the pond. It is this component that would induce convection currents in a freshwater pond thereby causing warm water to rise to the top where convection and evaporation would cause substantial heat loss. With proper concentration gradient, convection can be completely suppressed and significant heat collection at the bottom layer is possible. Salt gradient ponds are hydrodynamically stable if the following criterion is satisfied:

$$\frac{d\rho}{dz} = \frac{\partial\rho}{\partial s} \frac{ds}{dz} + \frac{\partial\rho}{\partial T} \frac{dT}{dz} > 0 \quad (49.37)$$

where s is the salt concentration, ρ is the density, T is the temperature, and z is the vertical coordinate measured positive downward from the pond surface. The inequality requires that the density must decrease upward.

Useful heat produced is stored in and removed from the lowest layer as shown in Fig. 49.21. This can be done by removing the bottom layer of fluid, passing it through a heat exchanger, and returning the cooled fluid to another point in the bottom layer. Alternatively, a network of heat-removal pipes can be placed on the bottom of the bond and the working fluid passed through for

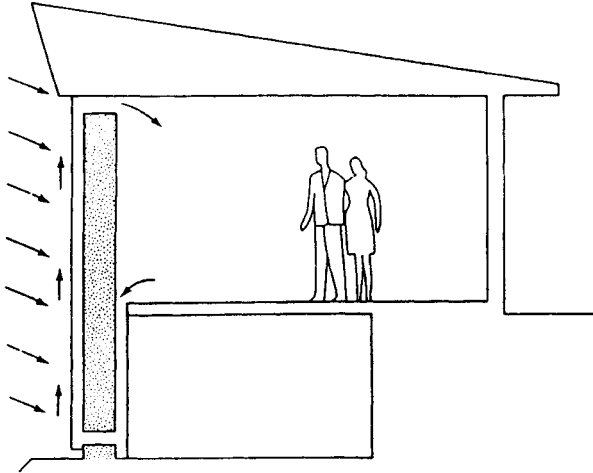


Fig. 49.19 Indirect-gain passive system—TSW system.

heat collection. Depending on the design, solar ponds also may contain substantial heat storage capability if the lower convective zone is relatively thick. This approach is used when uniform heat supply is necessary over a 24-hr period but solar flux is available for only a fraction of the period. Other convection-suppression techniques and heat-removal methods have been proposed but not used in more than one installation at most.

The requirements for an effective solar pond installation include the following. Large amounts of nearly free water and salt must be available. The subsoil must be stable in order to minimize changes in pond shape that could fracture the waterproof liner. Adequate solar flux is required year around; therefore, pond usage is confined to latitudes within 40° of the equator. Freshwater aquifers used for potable water should not be nearby in the event of a major leak of saline water into the groundwater. Other factors include low winds to avoid surface waves and windblown dust collection within the pond (at the neutral buoyancy point), low soil conductivity (i.e., low water content) to minimize conduction heat loss, and durable liner materials capable of remaining leakproof for many years.

The principal user of solar ponds has been the country of Israel. Ponds tens of acres in size have been built and operated successfully. Heat collected has been used for power production with an organic Rankine cycle, for space heating, and for industrial uses. A thorough review of solar pond technology is contained in Ref. 6. A method for predicting the performance of a solar pond is presented in the next section. The theory of pond optics, heat production, and heat loss is contained in Ref. 1.

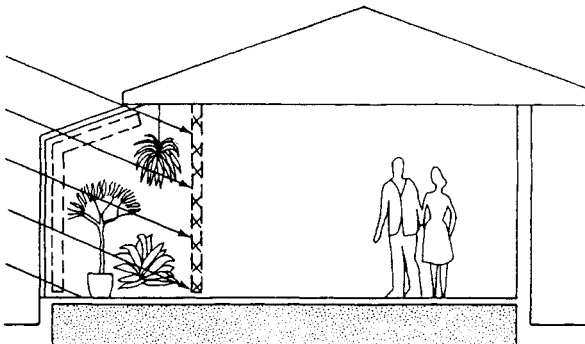


Fig. 49.20 Greenhouse or attached sun-space passive heating system using a combination of direct gain into the greenhouse and indirect gain through the thermal storage wall, shown by cross-hatching, between the greenhouse and the living space.

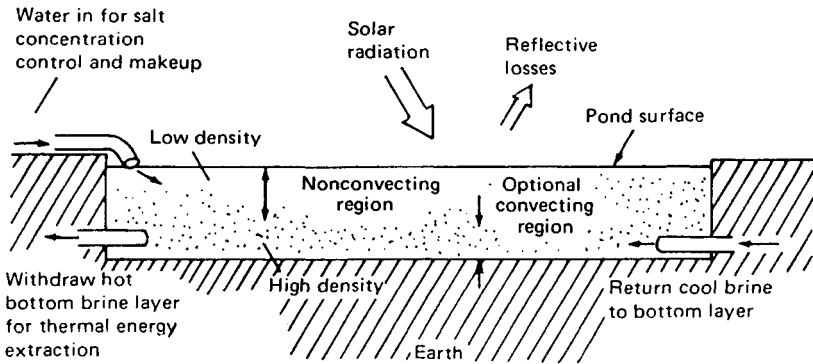


Fig. 49.21 Schematic diagram of a nonconvecting solar pond showing conduits for heat withdrawal, surface washing, and an optional convecting zone near the bottom.

49.3.5 Industrial Process Applications

Process heat up to 300°C for industry can be produced by commercially available trough-type concentrators. Most of the heat needed in the chemical, food processing, textile, pulp and paper, and petrochemical industries can, therefore, be provided by solar heat, in principle. In the United States about half of industrial heat is used at temperatures below 300°C. The viable applications below 300°C use collectors ranked in increasing temperature capability—flat-plates, solar ponds, evacuated tubes, and parabolic or other trough designs. Above 300°C, solar applications have been few in the major industries—primary metals, stone-lay-glass, electric power production.

Since many industrial processes operate around the clock, it may appear prudent at first glance to use substantial storage to permit high daily and annual load factors. This is appropriate from a thermal viewpoint but economic constraints have dictated that the most cost effective systems built to date have only sufficient storage to carry through solar transients of no longer than 30 min. The difficulty is the unavailability of an inexpensive, high-temperature, storage medium with proper heat-transport properties.

Solar industrial process heat was not yet a mature technology in the mid-1990s. Less than 100 systems existed worldwide and many of the earliest systems performed well below expectations. The key reasons were poor control function, lower than expected collector efficiency, parasitic heat losses in extensive piping networks, and poor durability of important components. However, the early experiments were very valuable in significantly improving this new technology. Later generation systems worked well, and the promise of solar heat applications is good under certain conditions of available land area for large arrays, adequate solar flux, and favorable economic conditions—advantageous tax consideration and expensive, nonsolar fuels. Significant reductions in system cost are needed for widespread application.

49.3.6 Solar Thermal Power Production

Solar energy has very high thermodynamic availability owing to the high effective temperature of the source. Therefore, production of shaft power and electric power therefrom is thermodynamically possible. Two fundamentally different types of systems can be used for power production: (1) a large array of concentrating collectors of several tens of meters in area connected by a fluid or electrical network and (2) a single, central receiver using mirrors distributed over a large area but producing heat and power only at one location. The determination of which approach is preferred depends on required plant capacity. For systems smaller than 10 MW the distributed approach appears more economical with existing steam turbines. For systems greater than 10 MW, the central receiver appears more economical.⁷ However, if highly efficient Brayton or Stirling engines were available in the 10–20 kW range, the distributed approach would have lowest cost for any plant size. Such systems will be available by the year 2000.

The first U.S. central receiver began operating in the fall of 1982. Located in the Mojave Desert, this 10-MW plant (called “Solar One”) is connected to the southern California electrical grid. The collection system consists of 1818 heliostats totaling 782,000 ft² in area. Each 430 ft² mirror is computer controlled to focus reflected solar flux onto the receiver located 300 ft above the desert floor. The receiver is a 23-ft diameter cylinder whose outer surface is the solar absorber. The absorbing surface is coated with a special black paint selected for its reliability at the nominal 600°C operating temperature. Thermal storage consisting of a mixture of an industrial heat transfer oil for heat transport and of rock and sand has a nominal operating temperature of 300°C. Storage is used

to extend the plant operating time beyond sunset (albeit at lower turbine efficiency) and to maintain the turbine, condenser, and piping at operating temperatures overnight as well as to provide startup steam the following morning. The plant was modernized in 1996.

Solar-produced power is not generally cost effective currently. The principal purpose of the Solar One experiment and other projects in Europe and Japan is to acquire operating experience with the solar plant itself as well as with the interaction of solar and nonsolar power plants connected in a large utility grid. Extensive data collection and analysis will answer questions regarding long-term net efficiency of solar plants, capacity displacement capability, and reliability of the new components of the system—mirror field, receiver, and computer controls.

49.3.7 Other Thermal Applications

The previous sections have discussed the principal thermal applications of solar energy that have been reduced to practice in at least five different installations and that show significant promise for economic displacement of fossil or fissile energies. In this section two other solar-conversion technologies are summarized.

Solar-powered cooling has been demonstrated in many installations in the United States, Europe, and Japan. Chemical absorption, organic Rankine cycle, and desiccant dehumidification processes have all been shown to be functional. Most systems have used flat-plate collectors, but higher coefficients of performance are achievable with mildly concentrating collectors. References 1, 2, and 8 describe solar-cooling technologies. To date, economic viability has not been generally demonstrated, but further research resulting in reduced cost and improved efficiency is expected to continue.

Thermal energy stored in the surface layers of the tropical oceans has been used to produce electrical power on a small scale. A heat engine is operated between the warmest layer at the surface and colder layers several thousand feet beneath. The available temperature difference is of the order of 20°C, therefore, the cycle efficiency is very low—only a few percent. However, this type of power plant does not require collectors or storage. Only a turbine capable of operating efficiently at low temperature is needed. Some cycle designs also require very large heat exchangers, but new cycle concepts without heat exchangers and their unavoidable thermodynamic penalties show promise.

49.3.8 Performance Prediction for Solar Thermal Processes

In a rational economy the single imperative for use of solar heat for any of the myriad applications outlined heretofore must be cost competitiveness with other energy sources—fossil and fissile. The amount of useful solar energy produced by a solar-conversion system must therefore be known along with the cost of the system. In this section the methods usable for predicting the performance of widely deployed solar systems are summarized. Special systems such as the central receiver, the ocean thermal power plant, and solar cooling are not included. The methods described here require a minimum of computational effort, yet embody all important parameters determining performance.

Solar systems are connected to end uses characterized by an energy requirement or “load” L and by operating temperature that must be achievable by the solar-heat-producing system. The amount of solar-produced heat delivered to the end use is the useful energy Q_u . This is the net heat delivery accounting for parasitic losses in the solar subsystem. The ratio of useful heat delivered to the requirement L is called the “solar fraction” denoted by f_s . In equation form the solar fraction is

$$f_s = \frac{Q_u}{L} \quad (49.38)$$

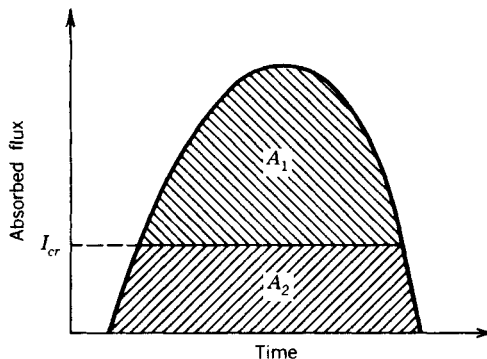


Fig. 49.22 Daily absorbed solar flux ($A_1 + A_2$) and useful solar flux (A_1) at intensities above I_{cr} .

Table 49.7 Empirical Solar Fraction Equations^a

System Type	f_s Expression	Time Scale
Water heating and liquid-based space heating	$f_s = 1.029P_s - 0.065P_L - 0.245P_s^2 + 0.0018P_L^2 + 0.00215P_s^3$	Monthly
Space heating—air-based systems	$f_s = 1.040P_s - 0.065P_L - 0.159P_s^2 + 0.00187P_L^2 + 0.0095P_s^3$	Monthly
Passive direct gain	$f_s = PX + (1 - P)(3.082 - 3.142\bar{\phi})(1 - e^{-0.329x})$	Monthly
Passive storage wall	$f_s = Pf_\infty + 0.88(1 - P)(1 - e^{-1.26f_\infty})$	Monthly
Concentrating collector systems	$f_s = F_R \bar{\eta}_0 \bar{A}_c \bar{N} \bar{\phi}' / L$	Monthly
Solar ponds (pond radius R to provide annual pond temperature \bar{T}_p)	$R = \frac{2.2 \bar{\Delta T} + [4.84(\Delta T)^2 + \bar{L}(0.3181 \bar{I}_p - 0.1592\Delta T)]^{1/2}}{\bar{I}_p - 0.5\Delta T}$	Annual

^aSee Table 49.8 for symbol definitions.

Empirical equations have been developed relating the solar fraction to other dimensionless groups characterizing a given solar process. These are summarized shortly.

A fundamental concept used in many predictive methods is the solar “utilizability” defined as that portion of solar flux absorbed by a collector that is capable of providing heat to the specified end use. The key characteristic of the end use is its temperature. The collector must produce at least enough heat to offset losses when the collector is at the minimum temperature T_{min} usable by the given process. Figure 49.22 illustrates this idea schematically. The curve represents the flux absorbed over a day by a hypothetical collector. The horizontal line intersecting this curve represents the threshold flux that must be exceeded for a net energy collection to take place. In the context of the efficiency equation [Eq. (49.32)], this critical flux I_{cr} is that which results in a collector efficiency of exactly zero when the collector is at the minimum usable process temperature T_{min} . Any greater flux will result in net heat production. From Eq. (49.32) the critical intensity is

$$I_{cr} = \frac{U_c(T_{min} - T_a)}{\tau\alpha} \tag{49.39}$$

The solar utilizability is the ratio of the useful daily flux (area above I_{cr} line in Fig. 49.22) to the total absorbed flux (area $A_1 + A_2$) beneath the curve. The utilizability denoted by ϕ is

$$\phi = \frac{A_1}{A_1 + A_2} \tag{49.40}$$

This quantity is a solar radiation statistic depending on I_{cr} , characteristics of the incident solar flux and characteristics of the collection system. It is a very useful parameter in predicting the performance of solar thermal systems.

Table 49.7 summarizes empirical equations used for predicting the performance of the most common solar-thermal systems. These expressions are given in terms of the solar fraction defined above and dimensionless parameters containing all important system characteristics. The symbols used in this table are defined in Table 49.8. In the brief space available in this chapter, all details of these prediction methodologies cannot be included. The reader is referred to Refs. 1, 4, 9, 10, and 11 for details.

49.4 NONTHERMAL SOLAR ENERGY APPLICATIONS

In this section the principal nonthermal solar conversion technology is described. Photovoltaic cells are capable of converting solar flux directly into electric power. This process, first demonstrated in the 1950s, holds considerable promise for significant use in the future. Major cost reductions have been accomplished. In this section the important features of solar cells are described.

Photovoltaic conversion of sunlight to electricity occurs in a thin layer of semiconductor material exposed to solar flux. Photons free electric charges, which flow through an external circuit to produce useful work. The semiconductor materials used for solar cells are tailored to be able to convert the majority of terrestrial solar flux; however, low-energy photons in the infrared region are usually not usable. Figure 49.23 shows the maximum theoretical conversion efficiency of seven common mate-

Table 49.8 Definition of Symbols in Table 49.7

Parameters	Definition	Units ^a
P_L	$P_s = \frac{F_{hx} F_R U_c (T_r - \bar{T}_a) \Delta t}{L}$	None
F_{hx}	$F_{hx} = \left\{ \left[1 + \frac{F_R U_c A_c}{(\dot{m} C_p)_c} \right] \left[\frac{(\dot{m} C_p)_c}{(\dot{m} C_p)_{\min} \epsilon} - 1 \right] \right\}^{-1}$ collector heat exchanger penalty factor	None
$F_R U_c$	Collector heat-loss conductance	Btu/hr · ft ² · °F
A_c	Collector area	ft ²
$(\dot{m} C_p)_c$	Collector fluid capacitance rate	Btu/hr · °F
$(\dot{m} C_p)_{\min}$	Minimum capacitance rate in collector heat exchanger	Btu/hr · °F
ϵ	Collector heat-exchanger effectiveness	None
T_r	Reference temperature, 212°F	°F
\bar{T}_a	Monthly averaged ambient temperature	°F
Δt	Number of hours per month	hr/month
L	Monthly load	Btu/month
P_s	$P_s = \frac{F_{hx} F_R \bar{\tau} \bar{\alpha}_c N}{L}$	None
$F_R \bar{\tau} \bar{\alpha}_c$	Monthly averaged collector optical efficiency	None
\bar{I}_c	Monthly averaged, daily incident solar flux	Btu/day · ft ²
N	Number of days per month	day/month
$(P'_L - \text{to be used for water heating only})$	$P'_L = P_L \frac{(1.18 T_{wo} + 3.86 T_{wi} - 2.32 \bar{T}_a - 66.2)}{212 - \bar{T}_a}$	None
T_{wo}	Water output temperature	°F
T_{wi}	Water supply temperature	°F
P_L	(See above)	None
P	$P = (1 - e^{-0.294Y})^{0.652}$	None
Y	Storage-vent ratio, $Y = \frac{C \Delta T}{\phi \bar{I}_c \tau \alpha_c A_c}$	None
C	Passive storage capacity	Btu/°F
ΔT	Allowable diurnal temperature saving in heated space	°F
$\bar{\phi}$	Monthly averaged utilizability (see below)	None
X	Solar-load ratio, $X = \frac{\bar{I}_c \tau \alpha_c N}{L}$	None
L	Monthly space heat load	Btu/month
f_∞	Solar fraction with hypothetically infinite storage, $f_\infty = \frac{\bar{Q}_i + L_w}{L}$	None
\bar{Q}_i	Net monthly heat flow through storage wall from outer surface to heated space	Btu/month
L_w	Heat loss through storage wall	Btu/month
$F_R \bar{\eta}_0$	Monthly averaged concentrator optical efficiency	None
$\bar{\phi}'$	Monthly average utilizability for concentrators	None
R	Pond radius to provide diurnal average pond temperature \bar{T}_p	m
ΔT	$\Delta \bar{T} = \bar{T}_p - \bar{T}_a$	°C
\bar{T}_p	Annually averaged pond temperature	°C
\bar{T}_a	Annually averaged ambient temperature	°C
\bar{L}	Annual averaged load at \bar{T}_p	W
\bar{I}_p	Annual averaged insolation absorbed at pond bottom	W/m ²

Table 49.8 (Continued)

Parameters	Definition	Units ^a
$\bar{\phi}$	Monthly flat-plate utilizability (equator facing collectors), $\bar{\phi} = \exp\{[A + B(R_N/R)](\bar{X}_c + C\bar{X}_c^2)\}$	None
A	$A = 7.476 - 20.0\bar{K}_T + 11.188\bar{K}_T^2$	None
B	$B = -8.562 + 18.679\bar{K}_T - 9.948\bar{K}_T^2$	None
C	$C = -0.722 + 2.426\bar{K}_T + 0.439\bar{K}_T^2$	None
\bar{R}	Tilt factor, see Eq. (49.21)	None
\bar{R}_N	Monthly averaged tilt factor for hour centered about noon (see Ref. 9)	None
\bar{X}_c	Critical intensity ratio, $\bar{X}_c = \frac{I_{cr}}{r_{T,N}\bar{R}_N\bar{H}_h}$	None
$r_{T,N}$	Fraction of daily total radiation contained in hour about noon, $r_{T,N} = r_{d,n}[1.07 + 0.025 \sin(h_{sr} - 60)]$	day/hr
	$r_{d,n} = \frac{\pi}{24} \frac{1 - \cos h_{sr}}{h_{sr} - h_{sr} \cos h_{sr}}$	day/hr
I_{cr}	Critical intensity [see Eq. (49.39)]	Btu/hr · ft ²
$\bar{\phi}'$	Monthly concentrator utilizability, $\bar{\phi}' = 1.0 - (0.049 + 1.49\bar{K}_T)\bar{X} + 0.341\bar{K}_T\bar{X}^2$ $0 < \bar{K}_T < 0.75$, $0 < \bar{X} < 1.2$	None
	$\bar{\phi}' = 1.0 - \bar{X}$ ($\bar{K}_T > 0.75$, $0 < \bar{X} < 1.0$)	
\bar{X}	Concentrator critical intensity ratio, $\bar{X} = \frac{U_c(T_{f,i} - \bar{T}_a)\Delta t_c}{\eta_0 I_c}$	None
$T_{f,i}$	Collector fluid inlet temperature—assumed constant	°F
Δt_c	Monthly averaged solar system operating time	hr/day

^aUSCS unit shown except for solar ponds; SI units may also be used for all parameters shown in USCS units.

rials used in the application. Each material has its own threshold band-gap energy, which is a weak function of temperature. The energy contained in a photon is $E = h\nu$. If E is greater than the band-gap energy shown in this figure, conversion can occur.

Figure 49.23 also shows the very strong effect of temperature on efficiency. For practical systems it is essential that the cell be maintained as near to ambient temperature as possible.

Solar cells produce current proportional to the solar flux intensity with wavelengths below the band-gap threshold. Figure 49.24 shows the equivalent circuit of a solar cell. Both internal shunt and series resistances must be included. These result in unavoidable parasitic loss of part of the power produced by the equivalent circuit current source of strength I_s . Solving the equivalent circuit for the power P produced and using an expression from Ref. 2 for the junction leakage I_j results in

$$P = [I_s - I_0(e^{e_0V/kT} - 1)]V \tag{49.41}$$

in which e_0 is the electron charge, k is the Boltzmann constant, and T is the temperature. The current source I_s is given by

$$I_s = \eta_0(1 - \rho_c)\alpha e_0 n_p \tag{49.42}$$

in which η_0 is the collector carrier efficiency, ρ_c is the cell surface reflectance, α is the absorptance of photons, and n_p is the flux density of sufficiently energetic photons.

In addition to the solar cell, complete photovoltaic systems also must contain electrical storage and a control system. The cost of storage presents another substantial cost problem in the widespread application of photovoltaic power production. The costs of the entire conversion system must be reduced by an order of magnitude in order to be competitive with other power sources. Vigorous research in the United States, Europe, and Japan has made significant gains in the past decade. The installed capacity of photovoltaic systems is expected to be at least 10,000 MW by the year 2000.

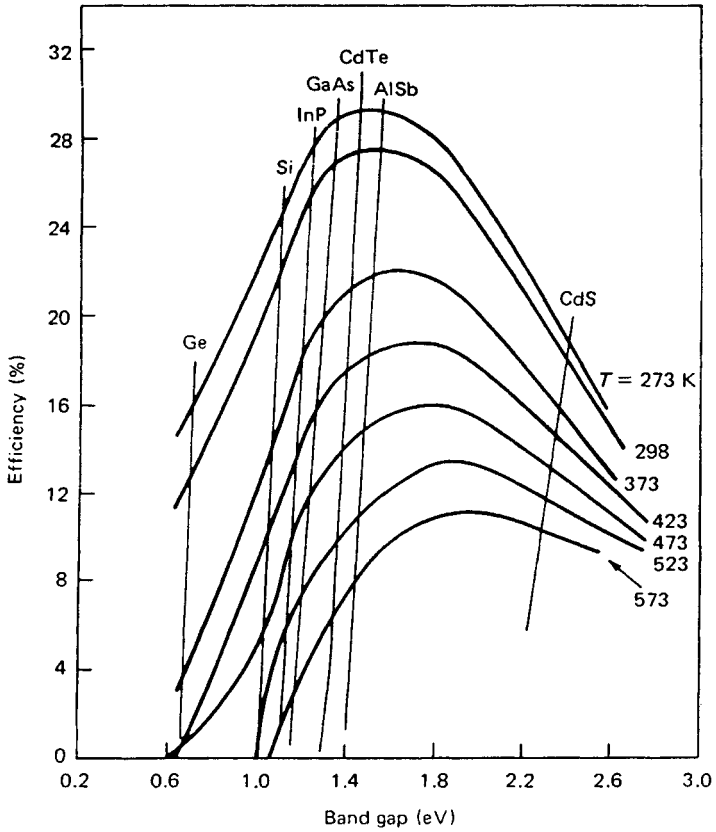


Fig. 49.23 Maximum theoretical efficiency of photovoltaic converters as a function of band-gap energy for several materials.

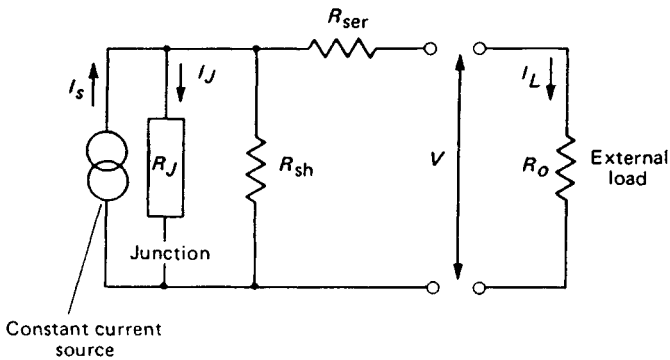


Fig. 49.24 Equivalent circuit of an illuminated *p-n* photocell with internal series and shunt resistances and nonlinear junction impedance R_J .

REFERENCES

1. J. F. Kreider and F. Kreith, *Solar Energy Handbook*, McGraw-Hill, New York, 1981.
2. F. Kreith and J. F. Kreider, *Principles of Solar Engineering*, Hemisphere/McGraw-Hill, New York, 1978.
3. M. Collares-Pereira and A. Rabl, "The Average Distribution of Solar Energy," *Solar Energy* **22**, 155–164 (1979).
4. J. F. Kreider, *Medium and High Temperature Solar Processes*, Academic Press, New York, 1979.
5. ASHRAE Standard 93-77, *Methods of Testing to Determine the Thermal Performance of Solar Collectors*, ASHRAE, Atlanta, GA, 1977.
6. H. Tabor, "Solar Ponds—Review Article," *Solar Energy* **27**, 181–194 (1981).
7. T. Fujita et al., *Projection of Distributed Collector Solar Thermal Electric Power Plant Economics to Years 1990–2000*, JPL Report No. DOE/JPL-1060-77/1, 1977.
8. J. F. Kreider and F. Kreith, *Solar Heating and Cooling*, Hemisphere/McGraw-Hill, New York, 1982.
9. W. A. Monsen, Master's Thesis, University of Wisconsin, 1980.
10. M. Collares-Pereira and A. Rabl, "Simple Procedure for Predicting Long Term Average Performance of Nonconcentrating and of Concentrating Solar Collectors," *Solar Energy* **23**, 235–253 (1979).
11. J. F. Kreider, *The Solar Heating Design Process*, McGraw-Hill, New York, 1982.